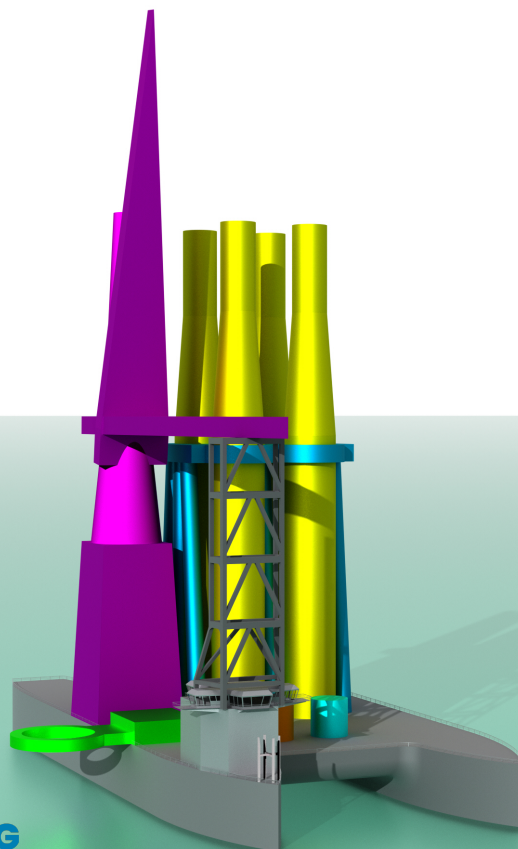# The design, production and verification of a fully elastic model of a catamaran
for hydroelastic experiments

A.M.E. Keser

October 4, 2023

Thesis for the degree of MSc in Marine Technology in the specialization
of *Ship and Offshore Structures* and *Ship Hydromechanics*

The design, production and verification of a fully elastic model of a catamaran

for hydroelastic experiments

by

A.M.E. Keser

Performed at

Vuyk engineering Rotterdam

This thesis MT.23/24.050.M is classified as confidential in accordance
with the general conditions for projects performed by the TUDelft.

October 11, 2023

Company supervisors
Responsible supervisor: Ir. A.J.H. Bot

Daily Supervisor(s): Ir. M. Verdult

Thesis exam committee
Chair/Responsible Professor: Dr. H.C. Seyffert
Staff Member: Dr. A. Grammatikopoulos
Staff Member: Dr. ir. J.H. den Besten
Company Member: Ir. M. Verdult

Author Details
Studynumber: 4686985

Abstract

Catamarans are popular in the offshore sector as they combine good transverse stability and ample deck space with low wave resistance. However, their slender hull shape results in low restoring qualities in heave and pitch motions. The large motions in rough weather can often result in water impacting the underside of the deck connecting the two hulls, a phenomenon called cross-deck slamming. The impulse excitation from cross-deck slamming can then produce a transient hydroelastic response of the structure called whipping. Whipping excites mode shapes that would not normally be present in the response, as their natural frequencies are significantly higher than the wave encounter frequency. This results in detrimental contributions to fatigue life through high-amplitude cyclical bending moments. Both the calculation of slamming loads and the prediction of resulting structural responses have been a challenge for several decades. The highly nonlinear and three-dimensional character of the phenomenon, combined with the strongly coupled fluid-structure interaction means that it is unpredictable, and even the definition of slamming events has been a matter of disagreement among researchers.

Experiments are still a vital part of these investigations, for validating ever-improving numerical techniques. An essential issue with experiments is the extent to which mode shapes and natural frequencies can be emulated in model scale. Traditional hydroelastic models are segmented and use either a flexible backbone or flexible joints to introduce stiffness. This often results in an excellent description of the 2-node bending mode, but an increasing error for higher modes leads to stress inaccuracies. In this investigation, a fully elastic model of a catamaran is designed and produced for hydroelastic experiments. The advantages and limitations of the concept are identified, and the verification against structural models is presented.

Preface

An end of an era.
With this thesis, I will not only close a chapter, I will close an entire book, that has been in the making for twenty years.

Growing up, I always loved water, sailing, and boats, which might also be because of my dad's job, who knows? So determined that I had made the right decision, I started this new chapter. And wow, what am I glad that I did. After three years, I finished my bachelor's and it wasn't a difficult decision to start the master Marine Technology.

Starting this graduation project was both exciting and frightening at the same time. However, against all my expectations, I actually enjoyed myself through it all, which I have many people to thank for.

First of all, I would like to thank my daily supervisors, who literally and figuratively helped me write this last chapter: First, Apostolos, who has taught me to question my decisions, but also accept that sometimes, the best decision is the least bad one, and equally as important, I want to thank Michiel, my daily supervisor at Vuyk, who gave me new insights from both practical applications and philosophical reasoning.

Secondly, I would like to thank everyone at the towing tank, specifically Jasper den Ouden, Peter Poot, and Sebastian Schreier, for helping with setting up the tests and building my model, and trusting me with all the very expensive equipment I got to use.

I also have my parents to thank, for their bottomless support and wisdom (and good genes), as well as my siblings, friends, and boyfriend, for putting up with me not being able to talk about anything other than my thesis for the past 9 months.

Lastly, I would like to thank Harleigh and Henk for being on my graduation committee and giving me constructive feedback to deliver an even better end result.

Anabel Keser
Delft, October 2023

Contents

List of Figures

List of Tables

Nomenclature

Abbreviations

COM	Centre of mass
LCG	Longitudinal centre of gravity
TCG	Transverse centre of gravity
VCG	Vertical centre of gravity
DIC	Digital image correlation
FEM	Finite element method
FRF	Frequency response function

Symbols

L	Length
B	Beam
D	Depth
T	Draft
Δ	Displacement
ρ	Density
E	Young's modulus
K	Bulk modulus
G	Shear modulus
ν	Poisson's ratio
λ	Scaling factor

1

Introduction

Catamarans are becoming more popular in the offshore installation sector due to their potential to execute more cost-effective and time-efficient installation methods [1]. The advantages of catamarans include their large deck area between its two hulls, which is catamaran-specific and can be used as work or storage space. Another advantage is their large transverse stability due to the large overall beam of the vessel, while the catamaran hulls can be relatively slender. These slender hulls have the advantage of leading to more design freedom when achieving streamlined hulls and they also reduce the wave resistance compared to monohulls with the same displacement.

However, these slender hulls also have the disadvantage that they lead to low restoring qualities when heaving and pitching. The wave damping is low due to the lack of longitudinal restoring properties which can lead to large relative motions, increasing the chance of slamming. Another disadvantage is that the cross-deck is subject to global loads, i.e. vertical bending moments, pitch connecting moments, and torsional moments, which are more significant than the global loads on a monohull due to the hull separation. But what is slamming?

1.1 Slamming

Kapsenberg, a researcher on the topic of slamming and whipping, gives a general definition for slamming:

> Slamming of ships is a phenomenon characterized by a high wave load of short duration. Usually the ships structure responds in a vibratory manner on this load; the response can be either a local or a global vibration mode or it can be in both modes together. These short duration loads are caused by large amplitude motions, even to the point that the fore body of the ship emerges from the water and slams upon re-entry, or they are caused by very steep waves that impact against the hull.
> The global elastic vibratory response of the structure is called whipping. It is characterized by a very low damping, so it takes many oscillations before it is extinguished. This dynamic response of the structure increases as well as the maximum load as the number of load cycles relevant for fatigue damage due to seakeeping loads. [2, p. iii]

Slamming is a hydroelastic problem, which is a form of fluid-structure interaction that deals with the interaction between water and elastic structures, in this case, ship structures. This is important only if it causes very high slamming pressures of a very short duration.

The reason slamming has been a popular topic of research is because it is one of the main sources of loading that need to be taken into account during the structural design [3]. This is because the slam responses can lead to large impulse loading on the structure of the ship. Locally this can result in plastic deformation of the structure, for example through buckling. Globally, it can cause whipping, which can significantly reduce fatigue life.

Investigations into the effect of slamming and whipping on the fatigue life of a catamaran, performed by Thomas et al., showed that the reduction of fatigue life due to the presence of slam events is significant: Structural locations show life reduction due to slamming between 55% and 61%. It was also shown that the estimated fatigue life reduces: 1) as the significant wave height increases, 2) as the frequency of slam occurrence increases, and 3) as the slam peak stress increases. [4]

1.2 Background on slamming research

Slamming investigations include analytical solutions, numerical simulations, and experimental research. Analytical formulations provide exact solutions for a simplified impact problem. Thus they are ideal to

use as benchmark tools for approximate methods and CFD methods. The analytical methods, in general, consist of a potential flow theory for estimating the hydrodynamics, coupled with a beam theory, for estimating the structural impact. Numerical simulations can be used to solve problems on more detailed and realistic structures. However, to obtain reliable and converged results for 3D slamming analysis, the fineness of the calculation meshes requires a lot of computation power, which can limit the application of this method.

Experimental research has been performed using three different methods: Full-scale trials, free-fall drop tests, and model testing. The use of full-scale sea trials has given a lot of valuable insight into the slamming behaviour of ships. Seeing how a real vessel reacts to certain loads and obtaining data has helped with the development of other analytical, numerical, and experimental techniques, and using the data as a comparison to those other techniques can lead to their validation. Full-scale trials also have disadvantages, namely that the process of relating the vessel's structural response to the obtained slamming response is difficult [5], the environmental conditions can't be controlled, and lastly, the trials are expensive and time-consuming.

A free-fall drop test is an experimental method where a 2D or 3D rigid body, mainly with a wedge shape, is pushed in the water, imitating a vessel that re-enters the water after an extreme heave or pitch motion. Because the drop test is a simplification of a complicated and highly nonlinear problem, they have been around for a long time. Even though the drop test has many advantages, such as the ability to obtain validation data for developing numerical methods, it was said by Shahraki that the experiments are not capable of modelling full 3D effects such as geometry, forward speed effects, dynamic vessel motions, and global vibrations [5]. Furthermore, whipping is not taken into account in drop tests.

Model testing is considered more realistic than free-fall drop tests, due to the ability to take into account the whole 3D geometry and environmental conditions [5]. A distinction can be made between rigid and hydroelastic models. As rigid models are not able to account for hydroelasticity, they will not be discussed here. In the next section, section 1.3, hydroelastic models will be discussed in more detail.

1.3 Current research

Three hydroelastic models can be used for hydroelastic model experiments: A segmented model with a flexible backbone, a segmented model with a flexible joint, or an elastic model.

The flexible backbone model is used most often and can have both a uniform cross-section and a non-uniform cross-section. When using a uniform cross-section, the 2-node longitudinal bending mode can be captured quite accurately, but the higher the number of nodes, the larger the error, leading to stress inaccuracies. Using the non-uniform cross-section does allow for accurately capturing more natural frequencies and mode shapes, however, this application is difficult and expensive.

Flexible joint models are also often used because the same sets of joints can be used to give the model a different uniform or distributed stiffness. This model, however, does not have a continuous structure and is therefore not able to capture the effects of cross-sectional characteristics. [6]
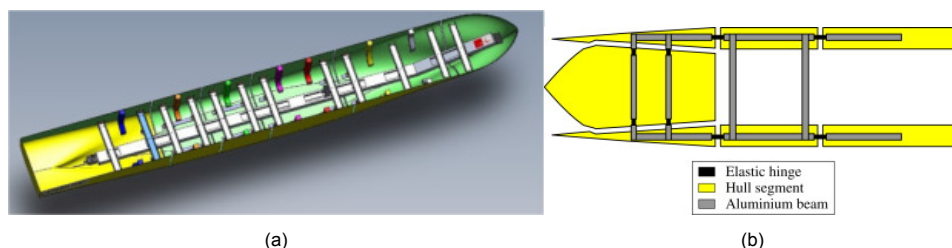
Figure 1.1: The two different segmented models. The subfigures show segmented models using (a) the flexible backbone [7] and (b) the flexible joint [8]

Elastic models are almost never used for hydroelastic experiments, as they are difficult to design and

produce. The scaling of the plating and stiffeners can lead to very small thicknesses, and once the scaling has been performed successfully, the manufacturing can be time-consuming and expensive. But, due to the developments in additive manufacturing, new production opportunities have appeared. In previous research, the first continuous model that closely resembled the detailed internal structure of a monohull (the so-called fully-elastic model) was designed, produced, and tested using additive manufacturing [9]. Using 3D modal testing, together with FEM, it was demonstrated that both global and local responses can be measured and the model can accurately emulate the mode shapes and natural frequencies.

The cross-deck of a catamaran is often significantly more flexible than the hulls, meaning that the transverse mode shapes can have natural frequencies that are lower than the longitudinal ones. An elastic model should be used to capture these transverse responses, as the segmented models described previously cannot capture this type of response.

1.4 Proposed research

The aim of this thesis is to investigate the design and production of a fully elastic model of a catamaran for hydroelastic experiments.

To capture the hydroelastic response of a reference vessel during model experiments, the model should have a mass distribution, bending stiffness, and natural properties representative of a reference vessel. Therefore, to accomplish the aim of this thesis, the following objectives will be performed:

1. Design a globally scaled model of a catamaran, including all primary members of the hull structure.

2. Produce the model out of polymer using additive manufacturing.

3. Plan and install instrumentation capable of capturing longitudinal and transverse responses.

4. Identify the modal properties of the structure and compare them to the numerical predictions.

Showing whether or not the proposed method is able to produce a model that is able to accurately emulate the mode shapes and natural frequencies of both transverse and longitudinal bending.

1.5 Design conditions

To set the scope for this thesis, design considerations are summarised and will be elaborated on in the chapters they have to be considered.

- Watertight and floating
- Produced with PETG
- Representative of the reference vessel
- Flume tank dimensions
- Printer dimensions and capabilities
- Instrumentation to capture responses

1.6 Methodology and research structure

To achieve the goal of this research, it is divided into two parts. In the first part, the fully elastic model is designed and produced and in the second part, modal properties are obtained with both model experiments and numerical experiments.

Figure 1.2 illustrates the structure of the research, which consists of the following chapters. Chapter 2 introduces the reference vessel, which has to be slightly simplified to obtain the full-scale model. In chapter 3, the scaling factor is selected, and the full-scale model is scaled down. Chapter 4 describes the design of a 3D model that supports additive manufacturing, which creates the production model. Finally, in chapter 5, the fully elastic model is created by 3D printing and assembling the production model.

Chapter 6 discussed the experimental method to obtain modal properties, the data acquisition techniques are discussed, as well as their setup. The obtained data is processed and the obtained modal properties are presented in chapter 7. Chapter 8 discusses the performed numerical modal analyses and, presents and discusses the obtained modal properties. The modal properties of both the model experiments and the numerical experiments are compared in chapter 9. The conclusions of the study are presented in chapter 10 and lastly, in chapter 11 recommendations are listed for future research.
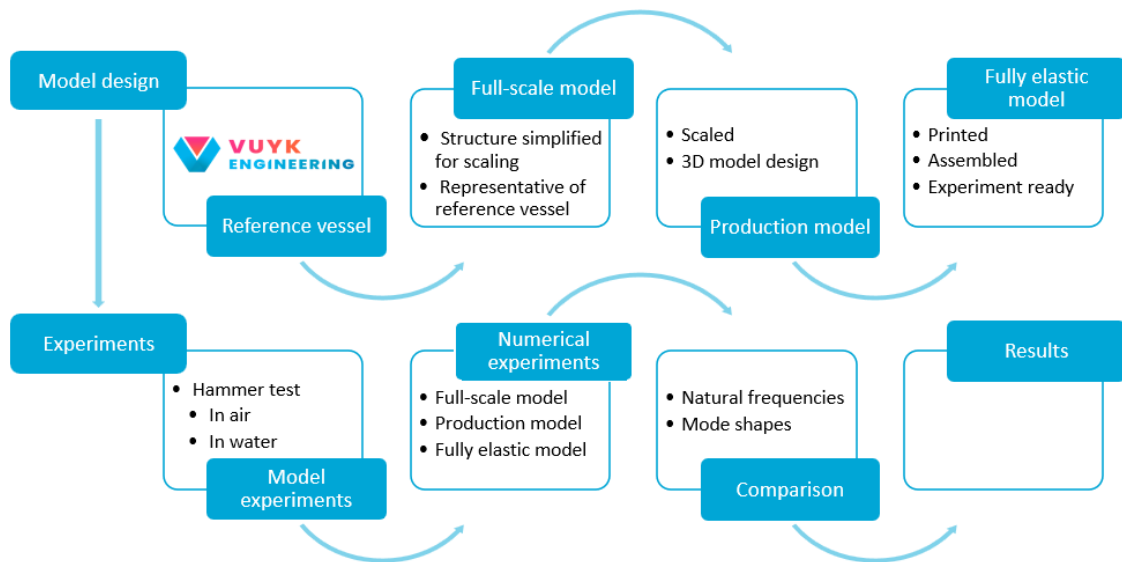
Figure 1.2: Schematics of the structure of this research.

2
Full-scale model

To obtain properly scaled hydroelastic responses of a vessel, the mass distribution, bending stiffness, and natural frequencies have to be representative of the reference vessel. Therefore, in this chapter, a full-scale model will be designed, based on a reference vessel provided by *Vuyk engineering Rotterdam*. This will be done by first discussing the reference vessel, and then discussing the full-scale model, together with the design approach.

2.1 Reference vessel

This section presents the vessel that is used as a reference for the full-scale model. The reference vessel is an offshore installation catamaran and has the principal particulars depicted in Table 2.1.

Table 2.1: Principal particulars of the full-scale vessel

Item	Value
L	198 m
B	90 m
D	26 m
T	10.5 m
Δ	84603.5 ton

Table 2.2 shows the mass distribution of the reference vessel. It should be noted that the lightweight also includes a large part of the deadweight masses, the detailed mass distribution can be found in Appendix A. The crane and main deck cargo make up the loading condition of the reference vessel. The construction drawing of the reference vessel can be found in Appendix B.

Table 2.2: Mass distribution of the reference vessel

Description	Weight [ton]	LCG [m]	TCG [m]	VCG [m]
Lightweight*	67384	99	0	14
Crane	7220	97	31	65
Cargo	10000	95	-23	71
Total	84604	98	0	25

This section discussed the principal particulars and mass distribution of the reference vessel, which will also be applied to the full-scale model. Now, the design of the full-scale model can begin, ensuring it can be scaled directly without requiring further adjustments to the internal structure, and thus maintaining a close resemblance to the reference vessel.

2.2 Full-scale model

In this section, the full-scale model will be designed, in a way that it can be directly scaled without needing further modification to the internal structure, which will ensure that the fully elastic model still resembles the reference vessel. The design criteria that have to be taken into account when designing the full-scale model are, that it has to 1) float, 2) be representative of the reference vessel and 3) be produced with PETG, which thus means that the model should be printable. The latter entailed that the internal structural detail had to be reduced slightly, without reducing structural strength.

First, the longitudinals (girders and stringers) are changed from tee stiffener to flat stiffener, then the number of web frames in between each bulkhead is reduced from three to one.

Then, the thickness of the structure has to be determined. The current structure, of the reference vessel, uses stiffeners to strengthen the hull plates to increase their load-absorbing capabilities and, thus minimize plate bending, however in the full-scale model, the stiffeners will be removed. To compensate for the strength of the stiffeners, the plate thickness has to be increased. First, this was done using the method of equivalent thicknesses, which calculates how much the thickness of the original plate has to increase for the plate bending to remain the same, when there are no stiffeners anymore. However, this method increased the thicknesses to such an extent, that the total mass of the structure, including loading condition, exceeded the displacement.

Thus, as it is crucial that the fully elastic model will float during experiments, it was decided to find a thickness that led to a total mass equal to the displacement, while still ensuring the first four mode shapes behave primarily globally. Which was obtained with a uniform thickness of 73 mm.

Table 2.3 presents the mass distribution of the full-scale model, designed to represent the reference vessel.

Description	Weight [ton]	LCG [m]	TCG [m]	VCG [m]
Steel structure	67442	96	0	14
Crane	7220	97	-31	65
Cargo	10000	95	23	71
Total	84662	96	0	25

Table 2.3: Mass distribution of the full-scale model

2.3 Conclusion

In this chapter, the reference vessel was introduced, highlighting its principal particulars and mass distribution, which serve as a foundation for the full-scale model. Implementing these parameters was one of the design criteria. The others emphasized the need for the full-scale model to float, to be scalable and to be produced using PETG.

The mass distribution of the full-scale model, detailed in Table 2.3, aligns with that of the reference vessel while maintaining primarily global behaviour in its first four mode shapes. Thus, it can be concluded that the full-scale model is suited to be scaled.

$\mathcal{3}$

Scaling

Scaling the full-scale model is the first step before being able to design or produce the fully elastic model. Therefore, a scaling factor (λ) has to be selected, which has to comply with multiple design criteria. The selected scaling factor will then be used to scale the principal particulars, mass distribution, and frequency of the full-scale model.

3.1 Scaling factor selection

In this section, it is discussed how the scaling factor is selected, which depends on various criteria. The design criteria entail that the model has to comply with
- the flume tank dimensions,
- the printer capacity and capabilities and,
- Experimental criteria.

Before the design criteria come into play, relations with respect to the scaling factor are discussed.

If Young's modulus (E) of the material should scale linearly with the scaling factor, and the second moment of area (I) of the cross-section with λ^4, then all thicknesses would also scale linearly. As this didn't seem possible due to the minimum printable thickness, it was decided to scale EI together with λ^5, see Equation 3.1. This led to more room to use the low material stiffness of PETG to design with higher thicknesses.

$$EI_m = \frac{EI_f}{\lambda^5} \tag{3.1}$$

The range of potential scaling factors, based on the size of the flume tank, was determined to be between 90 and 180. This range was then examined against the minimum printable thickness, which was determined to be two perimeters (in this case 0.56 mm). This was done by, numerically, performing modal analysis for the different potential scaling factors, with the goal of finding the scaling factors that showed that their first four mode shapes behave primarily globally, without going below the minimum thickness.

The first attempt indicated a scaling factor of λ = 130, with a uniform thickness of 0.84 mm, corresponding to 3 perimeters, which achieved a second moment of area very close to the original section with the non-uniform thickness. Although λ = 130 was viable from a structural perspective, the longest waves that could be generated in the flume would barely reach the ship-wave matching region. Consequently, it was decided to use a scaling factor λ = 180 instead. This significantly reduced the expected printing time as well and necessitated fewer splits along the breadth of the vessel to fit in the printer. The only concern was the structural strength of the new thickness which was equal to the minimum printable thickness, 0.56 mm. Initial test prints confirmed that this thickness was a viable option.

With the $\lambda = 180$, the principal particulars listed by Table 3.1, are obtained. The next section will discuss how the mass is properly scaled.

Table 3.1: Principal particulars after scaling with λ = 180.

Item	Value
L	1100 mm
B	500 mm
D	144.4 mm
T	58.3 mm

3.2 Mass

To correctly scale the mass, Equation 3.2 has to be used. By doing so, the target mass distribution, see Table 3.2, is obtained.

$$\Delta_m = \frac{\Delta_f}{\lambda^3} \tag{3.2}$$

Table 3.2: Target mass distribution

Description	Weight [kg]	LCG [mm]	TCG [mm]	VCG [mm]
PETG structure	11.6	528	0	139
Crane	1.24	539	-127	361
Cargo	1.71	128	128	394
Total	14.52	528	0	189

However, as Table 3.3 shows, the flexural modulus is not the only material difference between full-scale and model scale, as the density changes as well. As the density of PETG is approximately 7 times lower than the density of steel, there is a large decrease in the mass of the model's structure, compared to the target mass.

Table 3.3: Engineering data used in ANSYS for steel and PETG, where K and G are calculated according to E

Property	Steel	PETG	Unit
Density	7850	1180	kg/m^3
E	$2 \cdot 10^{11}$	$1.2 \cdot 10^9$	Pa
ν	0.3	0.3887	-
K*	$1.6667 \cdot 10^{11}$	$1.7969 \cdot 10^9$	Pa
G*	$7.6923 \cdot 10^{10}$	$4.3206 \cdot 10^8$	Pa

- Full-scale model: 67384 ton
- Target mass: 11.55 kg
- Obtained mass: 2.4 kg

The obtained mass is the mass of the scaled structure, made from PETG, and as discussed, this mass is significantly lower than the target mass. Therefore, ballast masses have to be added throughout the model in order to match the mass, centre of gravity, and natural frequencies with the target scaled values. The ballast masses are in the form of lead blocks, with an average mass of 250 grams. Figure 3.1 shows the distribution of the lead blocks added to the model, and Table 3.4 shows the location of the lead blocks.

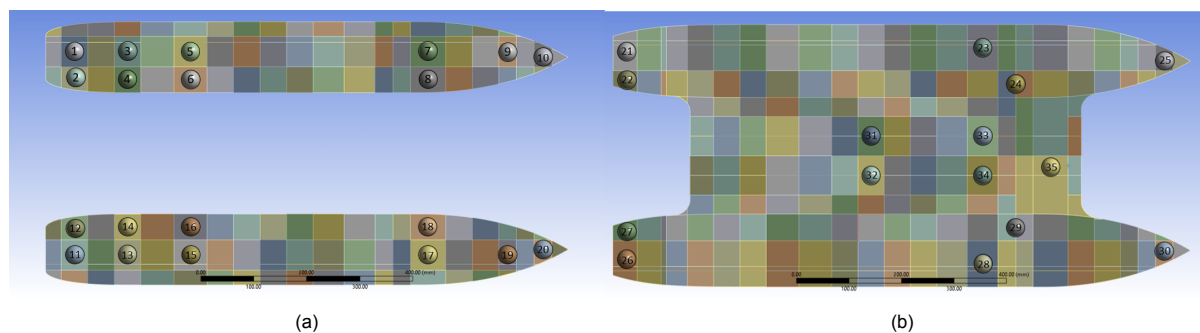(a)   (b)

Figure 3.1: The distribution of added lead masses. Subfigure (a) shows the masses on the bottom deck and Subfigure (b) shows the masses at the middle and cross deck.

Table 3.4: Locations of the lead blocks modelled inside of the structure using point masses.

Lead mass	x [mm]	y [mm]	z [mm]	Lead mass	x [mm]	y [mm]	z [mm]
1 & 11	167	±191	24	21 & 26	28	±196	95
2 & 12	167	±141	24	22 & 27	28	±146	95
3 & 13	267	±191	24	23 & 28	704	±206	95
4 & 14	267	±138	24	24 & 29	767	±137	95
5 & 15	385	±191	24	25 & 30	1050	±182	95
6 & 16	385	±138	24	31	492	38	115
7 & 17	833	±191	24	32	492	-38	115
8 & 18	833	±139	24	33	704	38	155
9 & 19	983	±190	24	34	704	-38	155
10 & 20	1050	±181	24	35	834	-22	155

By adding the 35 lead blocks, a total of around 8.75 kg mass is distributed over the model, and the mass distribution found in Table 3.5 was obtained. Comparing this mass distribution to the targeted mass distribution, Table 3.2, it can be seen that the weight difference is restored again. The mass distribution is highly influenced by the frequency, which will be discussed in the next section.

Table 3.5: Obtained mass distribution after adding lead blocks.

Description	Weight [kg]	LCG [mm]	TCG [mm]	VCG [mm]
PETG structure	2.4	532	0	80
Lead blocks	8.75	545	-1	56
Crane	1.24	539	-172	450
Cargo	1.71	528	128	394
Total	14.1	540	0	136

3.3 Frequency

In this section, it is explained what role the frequency has played during the scaling process. As discussed in the previous section, the lead blocks were added to match the obtained mass to the target mass. Determining the exact locations of the lead blocks was done using the modal analysis simulations in ANSYS. By moving around the lead blocks, the mass distribution changed, as well as the stiffness at certain locations, thus changing the natural frequencies. The used ANSYS model and the obtained natural frequencies are further discussed in chapter 8. The full-scale frequencies are scaled using Equation 3.3, leading to the target frequencies. The first four natural frequencies can be found in Table 3.6.

$$f_m = f_f \sqrt{\lambda} \tag{3.3}$$

The table lists the natural frequencies of the full-scale model, the calculated target values using Equation 3.3, and the obtained frequency after placing the lead blocks. As can be seen, the obtained natural frequencies from ANSYS agree well with the target natural frequencies.

Table 3.6: Natural frequencies full-scale model, target model (calculated), and scaled model from ANSYS.

Mode	Full-scale frequency [Hz]	Target frequency [Hz]	Numerical frequency [Hz]
1	1.322	17.736	17.919
2	1.494	20.044	20.733
3	2.475	33.206	33.492
4	2.600	34.883	35.337

3.4 Conclusion

After conducting numerical modal analysis, a scaling factor of λ = 180 was chosen. When the mass distribution full-scale model was scaled, it was found that lead blocks had to be added to compensate for the loss in weight due to the low density of the PETG. The lead blocks were added to match the

obtained frequency to the target frequency. While adding the lead blocks, the changes to the mass distribution and the natural frequencies could be monitored and influenced, however, it is unknown what the influence of the lead blocks is on the stiffness or the response of the model.

This approach ensured that after scaling, the model still resembled the characteristics of the full-scale model, and thus, it can be concluded that the scaling was done successfully, and thus a design can be made for the production model.

4
Production model

As the fully elastic model has to be produced out of polymer using additive manufacturing, the model for production (also referred to as production model) has to be designed to allow for this.

The main concern regarding the design of the production model is the manufacturing. Therefore, the main focus during the design process is the ability to both print and assemble the model, while the design criteria (section 1.5) are taken into account. The criteria applicable to the production model are regarding 1) printer dimensions, 2) instrumentation, and 3) has to be watertight.

As the printer dimensions are 24 cm by 20 cm by 20 cm, the model had to be split up into multiple segments to be assembled after printing. The vessel was split in transverse direction in three parts, namely the cross-deck and the two hulls. In the longitudinal direction, the model was split at every bulkhead and web frame (Figure 4.1c and Figure 4.1d), however, originally the longitudinal division was supposed to be at every bulkhead. To almost eliminate the need for support material, the web frame along with the longitudinals attached to it, was going to be printed separately from the main section, which would be printed from the bulkhead up, see Figure 4.1a and Figure 4.1b. The web frame would sit partly on the longitudinals of the main section and partly on a protruding perimeter. However, a test print revealed two significant caveats of this plan, which rendered it impossible. Firstly, the support for the web frame was insufficient, resulting in it not being securely attached in certain areas, which generated concerns for its structural integrity. Secondly, the main section had no internal structure for more than half of its length to hold the hull together, which resulted in severe buckling of the plating (Figure 4.2). Finally, drainage holes were added at multiple locations of each section, to allow draining of the model in case of leaks during testing in the flume.

To assemble the different sections, an overlapping system was designed: The whole model was printed with a double perimeter (0.56 mm). At each section, there was 1 cm, at both ends (front and back), where only one perimeter is printed. In the front, this is the outer perimeter and in the back, it is the inner perimeters, which means that, in theory, two successive sections slide together perfectly and can then be glued together using a thin layer of epoxy, which will also ensure no water leaking through.

The length of the overlap is not completely arbitrary. Before using an overlap length of a centimetre, a quarter of the length of a segment was used instead. However, this accentuated the buckling issues described previously. Figure 4.2 depicts buckling of such an overlap section - it should be emphasised

(a)   (b)

(c)   (d)
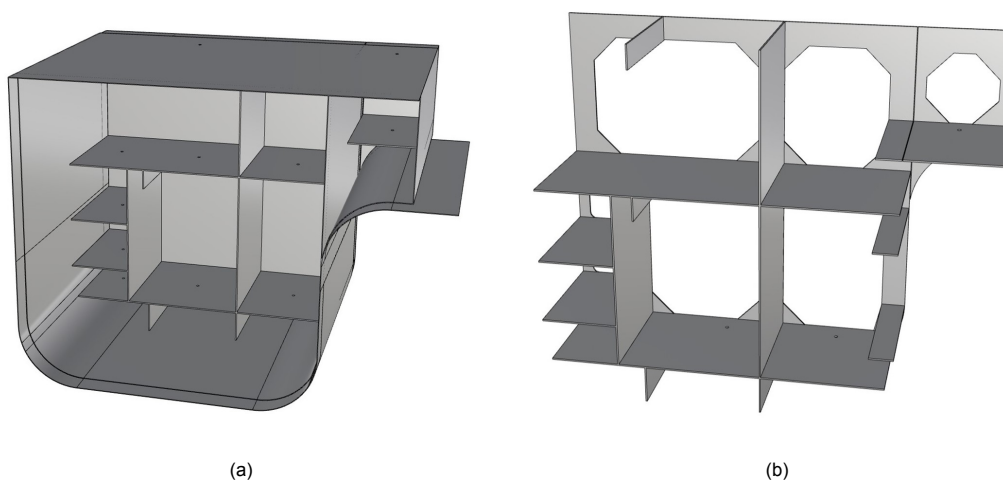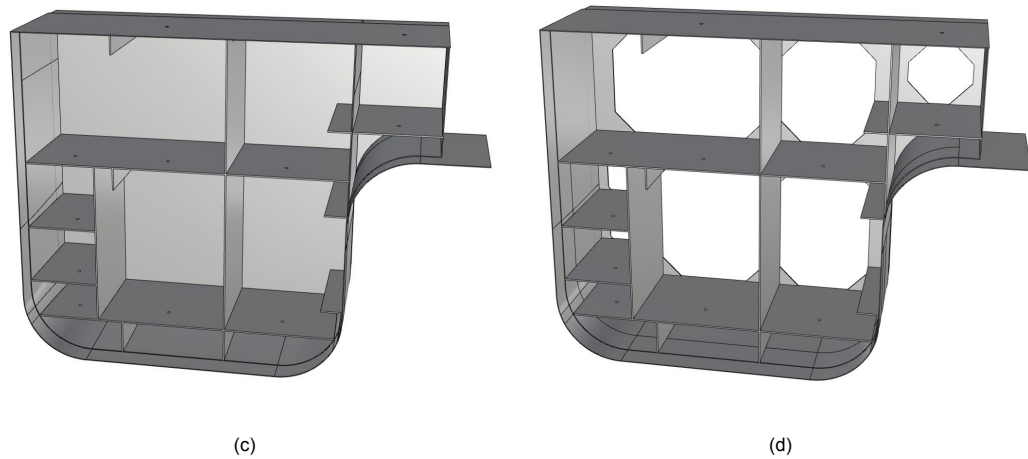
Figure 4.1: Longitudinal division of the model. Subfigures (a) and (b) depict the original design and Subfigures (c) and (d) depict the revised and final design.

that the whole in the middle is not a result of failure, but one of the drainage holes mentioned earlier, which is slightly malformed because of the buckling.
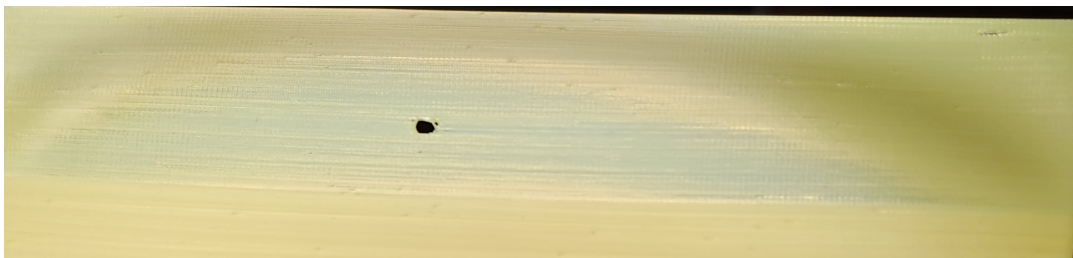
Figure 4.2: Buckling of the overlap section

Structures were designed for the crane and cargo to support the lead blocks that are needed in order to agree with the loading condition. Because resonance between the support structures and the total model has to be prevented, it is important that the crane and cargo resonance frequency is at least an order of magnitude larger than that of the full model. Therefore, static structural modal analyses are conducted in ANSYS on both support structures. In Figure 4.3 and Figure 4.4 both the design and the static structural analysis in ANSYS can be seen. It was found that with a thickness of 3 mm for both structures, the support structures both had resonance frequencies an order of magnitude larger than that of the full model, see Table 4.1.

Table 4.1: Natural frequencies of the model as a whole, the cargo support structure, and the crane support structure.

Mode	Model frequency [Hz]	Cargo frequency [Hz]	Crane frequency [Hz]
1	17.791	175	266
2	19.894	177	291
3	30.662	227	302
4	32.533	240	330
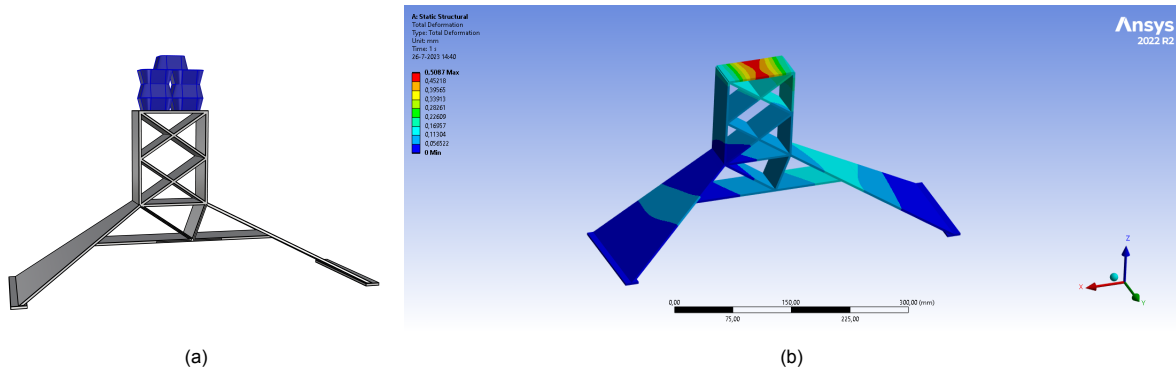
Figure 4.3: Design for the cargo support structure. Subfigure (a) shows the design in Rhino and (b) shows the static structural analysis in ANSYS.
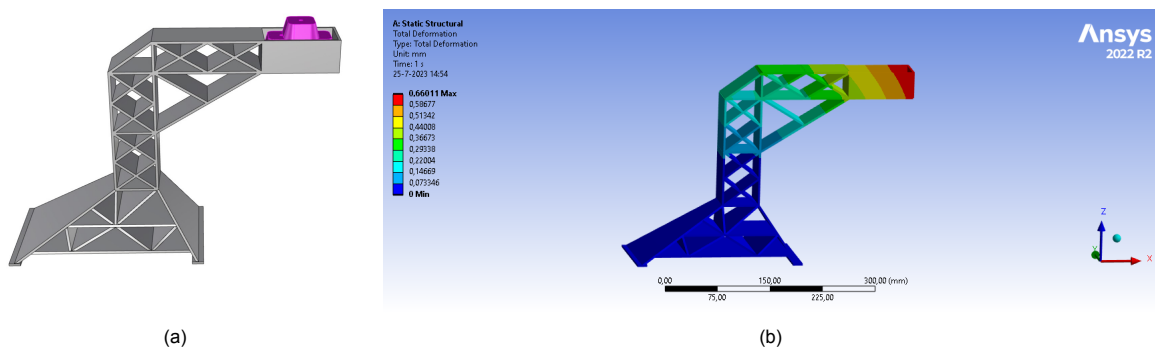
Figure 4.4: Design for the crane support structure. Subfigure (a) shows the design in Rhino and (b) shows the static structural analysis in ANSYS.

In order to measure the impact of the water on the cross-deck, pressure sensors will be used. The pressure sensors need to be removable and after adding the sensors, the model should remain watertight. To satisfy both criteria, the sensors, depicted in Figure 4.5a, were designed.
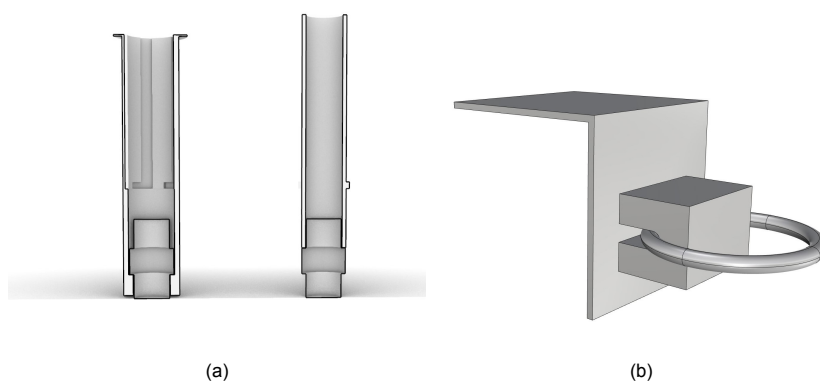
Figure 4.5: Designs of add-ons. Subfigure (a) shows the design for the pressure sensors, located in the cross deck of the model, and Subfigure (b) shows the design for the mooring line connections.

As the figure shows, the pressure sensor is enclosed by two tubes. The left tube is the outer tube and is attached to the cross-deck. The right tube, which is the inner tube that partly covers the sensor, is removable and can be locked in place using a locking system, also depicted in the figure. The outer tube has the same length as the cross deck, while the inner tube is 10 mm larger, which makes it pos-

sible to lock and unlock it.

Lastly, the mooring line connections are designed. As springs will be attached to these connections, they have to be able to withstand relatively high forces, and thus, they are designed to distribute the load over a larger area to minimise local behaviour. Figure 4.5b depicts the design of the mooring line connections, and as can be seen, it consists of three different components: two components made out of PETG that enclose a steel ring and are assembled using epoxy.

Table 4.2 shows the (calculated) mass distribution of the production model.

Table 4.2: Mass distribution of the production model

Description	Weight [kg]	LCG [mm]	TCG [mm]	VCG [mm]
Structure	2.11	532	0	80
Lead blocks	9.27	544	-0.6	57
Epoxy	0.42	531	0	86
Cargo	1.85	539	134	397
Cargo support structure	0.30	529	146	233
Crane	1.32	539	-172	400
Crane support structure	0.30	529	146	233
Total	15.89	534	-2.9	140

Now that the production model is designed while taking into account the printer dimensions, instrumentation requirements, and maintaining the watertight integrity, manufacturing of the model can start.

Fully elastic model

This chapter explains the manufacturing process of the fully elastic model. It starts with printing the production model, followed by the assembly of the print sections, Appendix C shows more pictures of the assembly. The finished result is the fully elastic model used for hydroelastic experiments.

5.1 Printing

The printing process will explained in this section. All structures were produced using the same printer, material, and set of parameters. A Prusa i3 MK3 printer was used, which was modified with a Bondtech extruder and an E3D 0.25 mm brass nozzle. The material used was eSUN PETG, which was maintained dry by being stored in an eSUN eBox Lite at a temperature of 50° C. During printing, the nozzle temperature was 230° C and the bed temperature was 80° C. The height of the first layer was 0.15 mm, and 0.125 mm for all other layers, whereas the extrusion width was set at 0.28 mm. All longitudinal components were printed using only perimeters, of which the external ones were printed at a speed of 35 mm/s, and the internal ones were printed at a speed of 65 mm/s. The bulkheads and web frames were printed with 100% rectilinear infill, at a speed of 30 mm/s.

All structures were printed with the longitudinal axis of the ship coinciding with the vertical axis of printing (layering direction). This decision was made as ships have a nearly prismatic geometry along the length, which can be printed very efficiently vertically. Since the vessel was split at each bulkhead and each web frame, these parts of the structure were printed first on the build plate, ensuring sufficient adhesion. Subsequently, the remainder of the section was printed with little to no need for support material.

Due to the small intended thickness, most of the longitudinal components of the model were printed with two perimeters of material, for an intended thickness of approximately 0.6 mm. At the locations where sections would be joined together, a single perimeter thickness was used, as the thickness was split between the two neighbouring sections to create an overlap at the joint. This meant that the first and last cm of each section only had a single perimeter. Similarly, the innermost parts of the hulls, where they would be connected to the cross-deck sections, also had a single-perimeter thickness. Unsurprisingly, these proved to be the areas of the structure featuring the most production issues. These included:
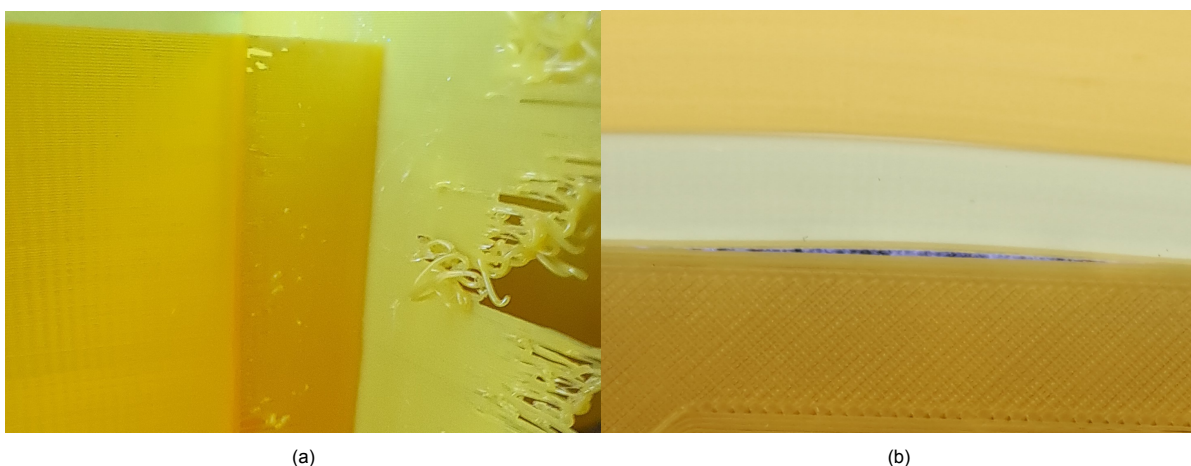

(a)　　　　　　　　　　　　　　　　　　　　　(b)

Figure 5.1: Common issues in areas of single-perimeter thickness: Subfigure (a) shows missing material near stiffeners (left) and poor printing of overhanging single-perimeter walls (right) and Subfigure (b) shows separation of side wall from bulkhead due to plate buckling.

1. Spots of "missing" material near the end of the sections close to the bulkhead or web frame. These were generated in areas where the printer started generating a perimeter at the location of a deck or stiffener (Figure 5.1a).

2. Separation between the longitudinal plating and bulkhead or web frame, in areas where the plating was prone to buckling (Figure 5.1b).

3. Poor printing of the single-perimeter plating at the areas connecting the hulls to the cross-deck. This was caused by a combination of the single-perimeter printing, the fact that the wall was generated on top of support material, and the fact that one of the ends was completely free (Figure 5.1a).

As would be expected, the single-perimeter areas were also significantly more sensitive than other regions and sometimes suffered further damage during handling. Issues described above either resulted in discarding and reprinting the section at hand or were repaired before use, depending on the severity. Judging from the behaviour of the neighbouring double-perimeter regions, it was concluded that most of these issues would have been absent if at least 2 perimeters were used everywhere. Single-perimeter thicknesses will be avoided in future iterations of 3D-printed fully elastic models.

After printing, the mass of each section was measured and compared to expectations, showing maximum deviations of up to 1-2%. The largest deviations consistently corresponded to some of the lighter sections, indicating that the accuracy of the scales used was partly to blame. Extensive thickness measurements (more than 30 for most sections) were also taken through each section. These indicated slightly higher values than anticipated: an average of 0.58 mm with a standard deviation of 0.04 mm. This is attributed to the way thicknesses are calculated and processed with slicing software for 3D printing, where two perimeters do not necessarily produce exactly double the thickness of a single perimeter. It should be pointed out that these measurements were all taken at various parts of the longitudinal structure. As the bulkheads and deep frames were all inaccessible, measurements were taken from scrap bulkheads and deep frames. From measurements, it followed that the web frames had an average thickness of 0.52 mm, and the bulkheads had also an average thickness of 0.58 mm. These measurements were taken from scrap bulkheads and deep frames, as the model had already been assembled. This process will be explained in the next section.

5.2 Assembly

After printing, the lead blocks were glued inside the structure using a black kit. The sections were joined using epoxy, and then waterproofing of the model was performed by applying two layers of epoxy externally. Testing this method on a small specimen with the same thickness demonstrated consistently watertight behaviour.

The exact thickness of the epoxy is very challenging to measure, so an approximation will be made. The epoxy increased the mass of the model by 140 g, over a surface area of $1415181.5\,mm^2$ and, according to the manufacturer [10], it has a density of $0.0011\,g/mm^3$, which leads to an approximated thickness of around $0.1\,mm$ and is expected to have a more significant effect on the stiffness.

The last part of the assembly is the waterline. By moving around the lead blocks intended for the crane and cargo, while the model was floating inside the water, the waterline could be matched up with the design waterline. The final mass distribution for the fully elastic model can be found in section 5.3.

During assembly, some difficulties were encountered due to the single-perimeter printing issues. The first issue encountered was that epoxy would have trouble adhering to the material printed near the end of the section that had gaps of "missing" material, as depicted in Figure 5.1a. Therefore, these pieces had to be cut off, leaving the bottom of the cross deck partly with only a single perimeter. As this problem occurred around the centre line of the whole bottom of the cross deck, it had to be filled with epoxy, ensuring enough strength.

The other issue that was encountered was due to the buckling of the single-perimeter at the overlapping section. Due to the buckling, gaps appeared between two sections at the overlapping area. Reinforce-

ments were added to the inside of a drying "section pair", pushing the overlap surface on the inside against the outside surface. As it is impossible to know for certain if the gaps are fully closed, and thus watertight, when filling them with epoxy, it is important to close as many gaps using the reinforcements.

(a)   (b)
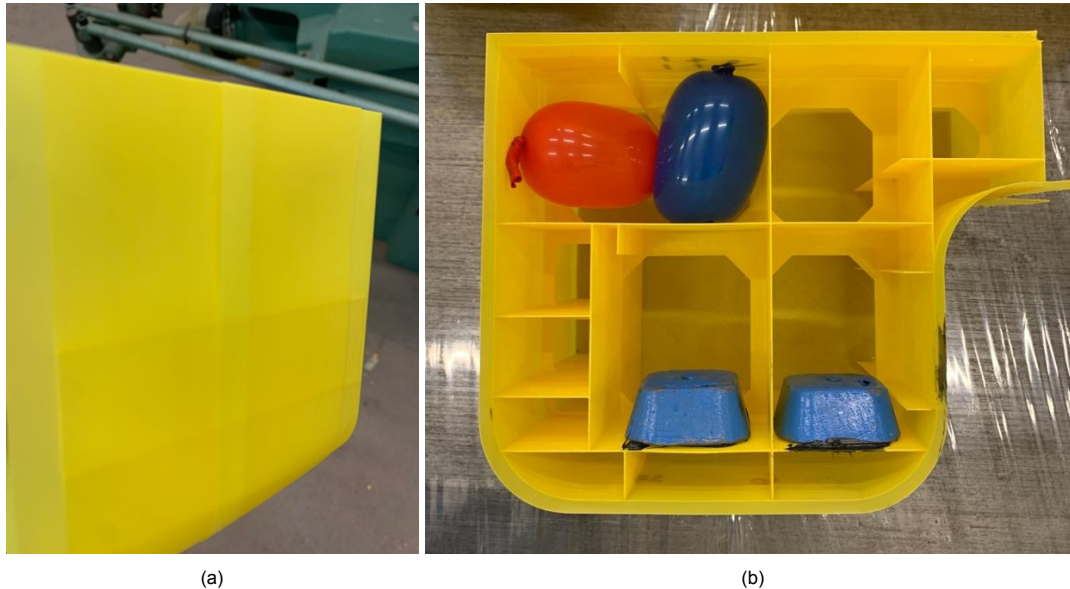
Figure 5.2: Encountered buckling problem. Subfigure (a) shows the gap between the two overlapping surfaces and Subfigure (b) shows the reinforcements used to solve the buckling.

5.3 Fully elastic model

Figure 5.3 depicts the fully elastic model after its completion. To ensure even keel, lead blocks from the crane are moved to the deck, which leads to a new mass distribution. During the assembly, the model was weighed; 1) before and after epoxy, 2) before and after support structures, and 3) when it was finished. This leads to the detailed mass distribution listed by Table 5.1.

Table 5.1: Mass distribution of the fully elastic model.

Description	Weight [kg]	LCG [mm]	TCG [mm]	VCG [mm]
PETG structure	2.11	532	0	80
Lead blocks	8.57	544	-0.6	57
Epoxy	0.14	531	0	86
Cargo	1.69	538	134	397
Cargo support structure	0.25	529	146	233
Crane	0.72	533	-172	392
Crane support structure	0.57	350	-175	259
Lead blocks on deck	0.48	878	-47	153
Total	14.52	544	0.7	131
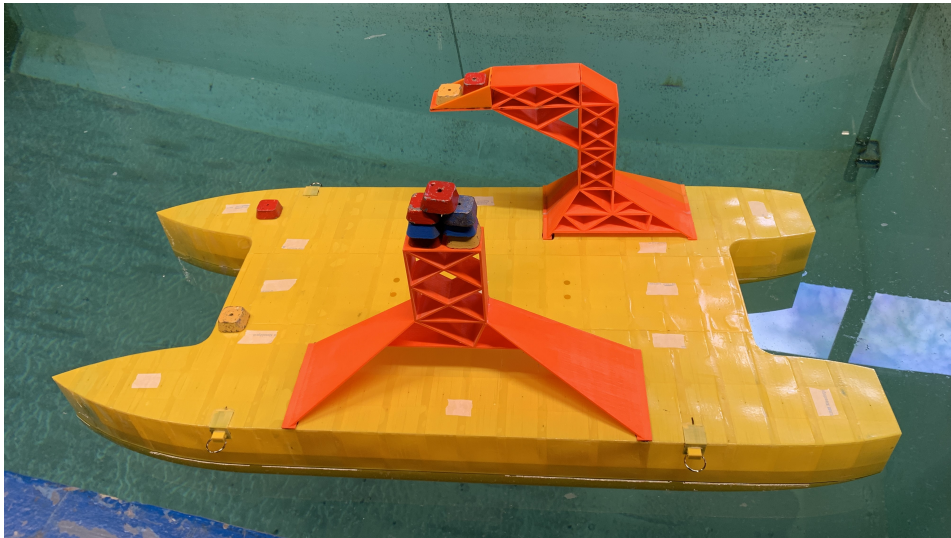
Figure 5.3: Fully elastic model after production.

5.4 Conclusion

In this chapter, the transformation of the production model into a fully elastic model is detailed, beginning with the printing process. Printing parameters and techniques were optimised, with specific attention to overcoming challenges in areas of single-perimeter thickness, which led to issues such as missing material, the separation between plating and frames, and poor printing quality. Nevertheless, the overall accuracy of the printed sections was maintained within acceptable tolerances. After printing, the model was assembled, and changes were made to the mass distribution to obtain the correct waterline for the model.

During assembly, some difficulties emerged, especially related to the single-perimeter printing issues, which required additional care and reinforcement to ensure structural integrity and watertightness. However, it was still possible to obtain a fully elastic model, that is suited for hydroelastic experiments.

6
Model experiments

In this chapter, the modal properties of the fully elastic model are determined. This is done by explaining 1) the experimental method used to perform modal experiments, 2) the measurement techniques that are used, and 3) the setups needed for the different measurement techniques.

6.1 Hammer testing

To perform a modal analysis, a hammer test can be used. By hitting the model with a soft hammer, and recording the oscillations and their decay, the natural frequencies and mode shapes can be obtained. In this research, two different types of instrumentation are used: Accelerometers and digital image correlation (DIC).

6.1.1 Accelerometers

When using accelerometers to measure the hammer impact, multiple sensors are needed over the target area. Both the number and the placement of the sensors are important to limit spatial aliasing, which is when mode shapes of a high frequency look similar to mode shapes with a lower frequency.

With the accelerometers, the vibrations of the structure after the hit are measured. The measurements are made with the data acquisition software DEWEsoft, which will use the accelerations (input) to return the frequency response. During post-processing, the frequency response can be used to plot the frequency response function (FRF), and the corresponding mode shapes.

6.1.2 DIC

DIC is an optical technique for measuring strain and displacement. High-speed full-field experimental data of structural deformations can be obtained. It is a non-contact process and it is good for flexible materials. It compares two images of a component before and after deformation. Displacements and strains are determined by correlating the position of pixel subsets in the original and deformed image, normally based on contrast, in this case, grey intensity levels.

Hydroelastic experiments were often performed using strain gauges to determine the strains and displacements of a structure. However, strain gauges will add stiffness, produce heat, and only obtain point measurements, usually in one direction, for very complicated mode shapes. As DIC is a non-contact technique, no additional stiffness or heat is added to the model, and it is capable of gathering both local and average data, more information on the structure is available.

Post-processing of the images is done using the software Istra4D. In this program, the images are imported, a mark and starting point are indicated, as well as setting the subset and grid space. The software uses the input (images) and returns the deformation in the time domain. In section 7.3 it is explained how the deformation in the frequency domain is obtained.

6.2 setup

To obtain a wide range of information on the natural properties, three different test setups are investigated. The first two setups, in air and in water, only make use of accelerometers and the last experiment is performed using both accelerometers and DIC. For all tests, the impact location is the horizontal area of the back leg of the support structure, as this is one of the few locations on the vessel where the hammer hit could be administered without risking local damage.

6.2.1 Hammer test in air

For the tests in air, the model had to be suspended to emulate free boundary conditions. Attaching springs on the top deck was not an option, again, due to the risk of local damage. Consequently, bot-

tom suspension was needed. Bungee cords were the first option, as used in previous tests with elastic models [11]. However, concerns were raised regarding the capability of the structure to withstand such concentrated pressure. Eventually, bicycle inner tubes were used instead, which combined low stiffness with a larger contact area.
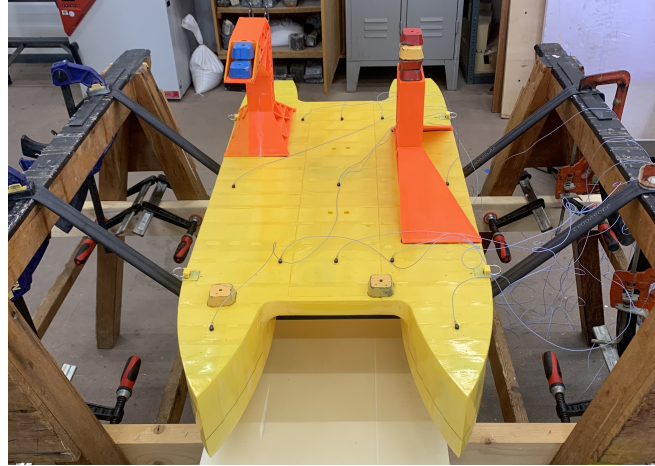
Figure 6.1: setup for the hammer testing in air.

Figure 6.1 depicts the final setup with the bicycle's inner tubes. The tubes are clamped between two trestles with the model on top. On the deck of the model, the accelerometers are placed, which can be seen in Figure 6.2 and the locations of the sensors can be found in Table 6.1, where x and y stand for the length and width of the model.

Figure 6.2: Accelerometer placements for modal experiment in air.

Table 6.1: Location of the accelerometers for the modal tests in both air and water.

Sensor	x [mm]	y [mm]
1	100	180
2	100	-180
3	200	0
4	200	90
5	200	-90
6	540	0
7	540	210
8	540	-210
9	790	0
10	790	90
11	790	-90
12	960	180
13	960	-180
14	430	55
15	430	-55

6.2.2 Hammer test in water

The hammer test is repeated in water, both for accelerometers only, and later also with both the accelerometers and the DIC. The test with accelerometers only, is performed on a 'free floating' model, see Figure 6.3a, making sure the model is not touching the wall of the water tank. The sensors are located the same as the hammer test in air, thus the same as in Table 6.1.
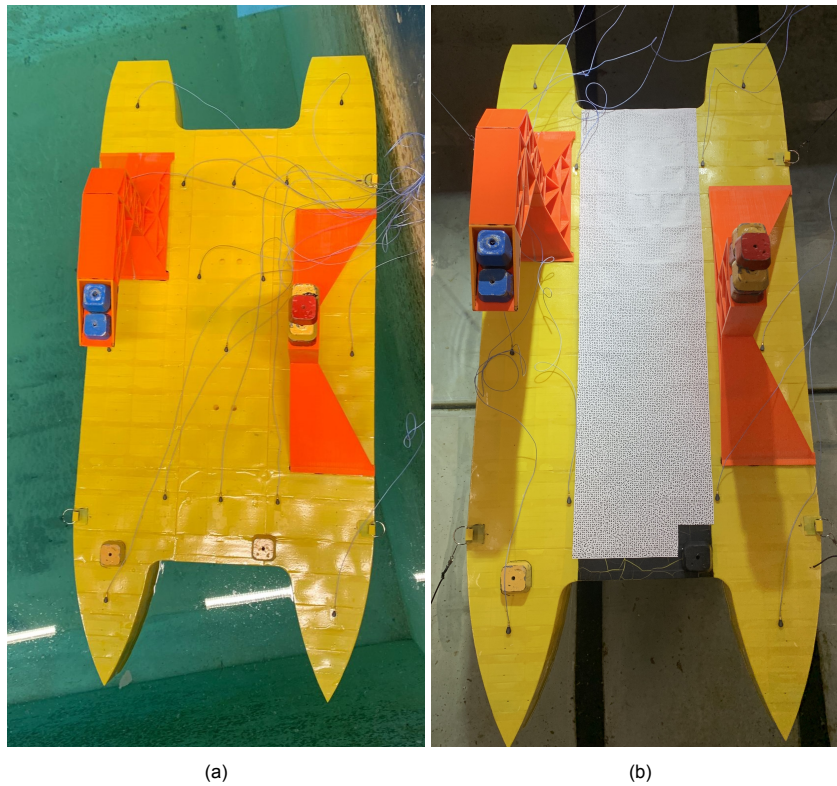
Figure 6.3: Accelerometer placement for modal experiments in water. Subfigure (a) shows the placement when only the accelerometers are used and Subfigure (b) shows the accelerometer configuration when it is combined with DIC.

The placement of the accelerometers when combined with the DIC is different than for the first two test configurations. Figure 6.3b shows a reduced number of accelerometers, which is due to the fact that the cross deck has to be empty for the speckle pattern. The location of the remaining sensors can be found in Table 6.2.

Sensor	x [mm]	y [mm]
1	100	180
2	100	-180
4	200	90
5	200	-90
7	540	210
8	540	-210
10	790	90
11	790	-90
12	960	180
13	960	-180

Table 6.2: Location of the accelerometers for the modal test combined with DIC.

6.2.3 DIC

The hammer test combining the accelerometers and the DIC is set up in the flume tank. First, the flume tank setup will be discussed, followed by the additions to the model needed to perform DIC measure-

ments.

Flume tank setup

Figure 6.4 illustrates the flume tank setup, which consists of two high-speed cameras, as these are able to capture the frequency range of interest. Both cameras are equipped with the same set of lenses, making sure their focus is on the cross deck of the model, which is the target area during the experiments.
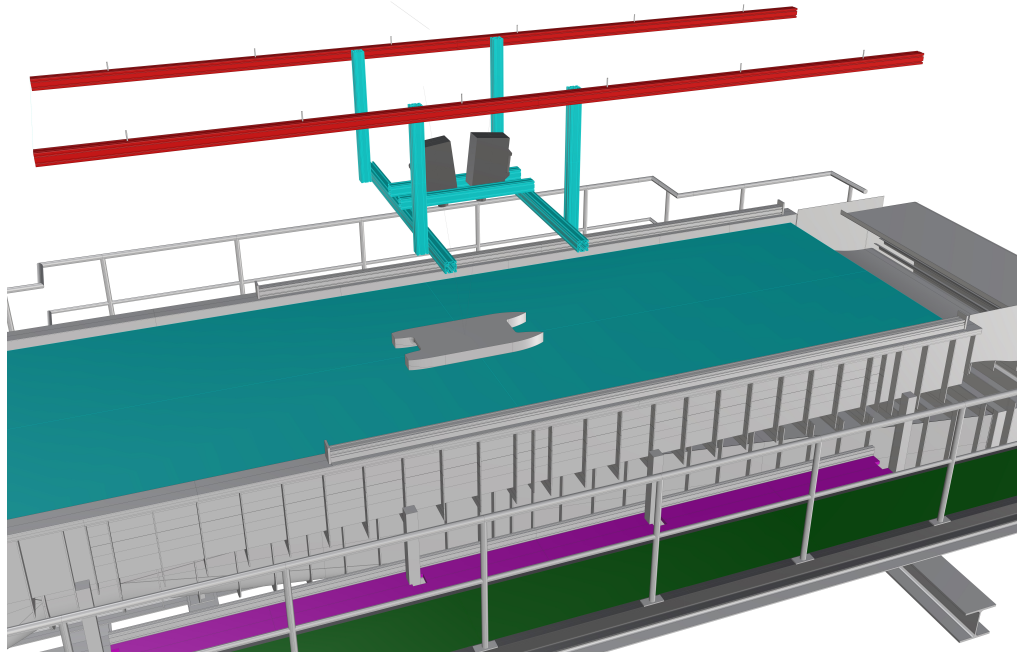
Figure 6.4: setup of the high-speed cameras in the flume tank for the DIC measurements.

Model setup

To successfully perform DIC measurements, the model has to be provided with a speckle pattern, that is picked up by the high-speed cameras. The speckle pattern is only applied to the cross deck, as this is the area of interest. A speckle pattern depends on the view of the camera, the distance between the camera and the specimen, and the pixels of the camera and is determined by the amount and size of the speckles. The speckle pattern should contain uniform speckles: They should be of the same size and the distance between the speckles should be more or less equal to the size of the speckles, leading to a black-and-white ratio of 50%.
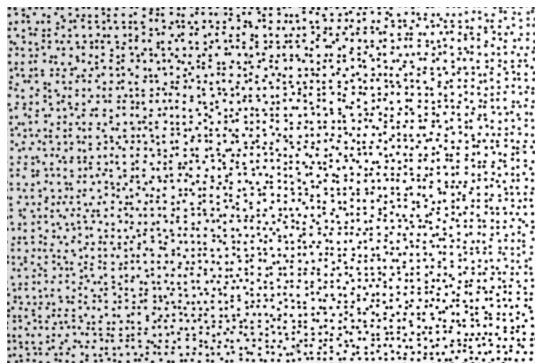
Figure 6.5: Selected speckle pattern for the DIC measurements

The selected speckle pattern, displayed by Figure 6.5, is printed on normal paper and glued on the cross deck of the model using CD glue.

Lastly, mooring lines are added to the model, to ensure that the model stays in the view of the cameras after it is hit with the hammer. Figure 6.6 shows the last hammer test setup, performed in the flume tank.
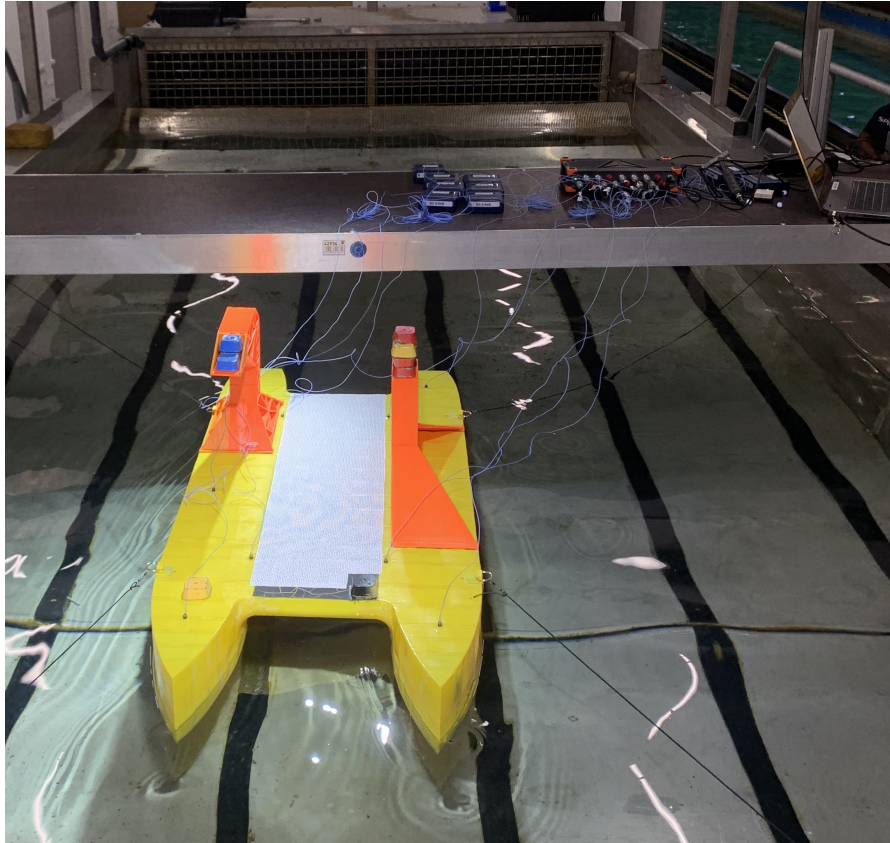
Figure 6.6: setup in the flume tank showing both the accelerometers and the additions for the DIC.

6.3 Conclusion

The chapter provides an overview of the experimental methodology, measurement techniques, and setups used to obtain the natural properties of the fully elastic model. This information is essential for understanding how the modal experiments were conducted and how the data for subsequent analysis were collected, thus making sure the data can be processed correctly.

Results of the model experiments

In this chapter, data will be processed, and modal properties will be obtained and discussed. First, the accelerometer data obtained in water will be discussed, followed by the accelerometer data in air and lastly, the data obtained with DIC measurements will be discussed.

7.1 Accelerometers in water

This section presents the results obtained with accelerometers in water but first discusses the data processing, which is the same for both accelerometers in water and in air.

As discussed in subsection 6.1.1, the data is obtained as well as processed by acquisition software DEWEsoft. From DEWEsoft, the output can be exported for each sensor in the form of the amplitude in $m/s^2/N$. As the frequency response is a complex function, it consists of a real part and an imaginary part. The FRF is plotted using the imaginary part of the amplitude. The mode shapes are plotted after the data is normalised with respect to measurements from sensor 1, leading to the results discussed in this section.
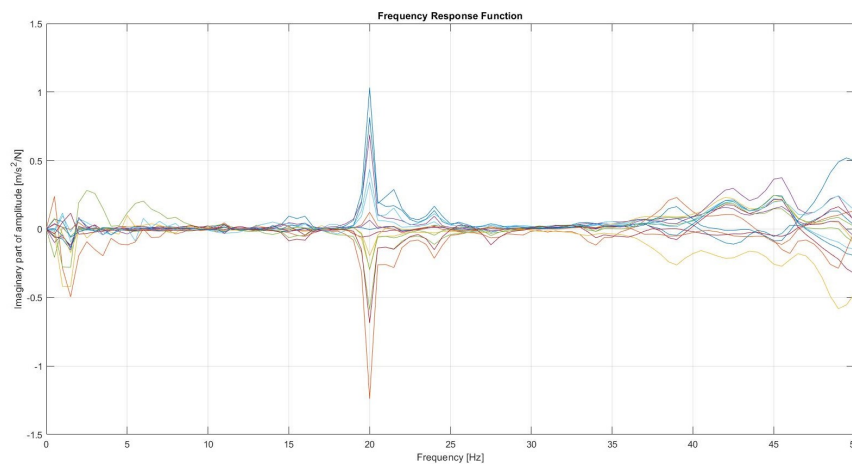
Figure 7.1: FRF of the configuration in water

Figure 7.1 illustrates the presence of resonance peaks at the frequencies listed below, that have corresponding mode shapes that can be found in Figure 7.2.

- 20 Hz
- 24 Hz
- 39 Hz
- 42.5 Hz
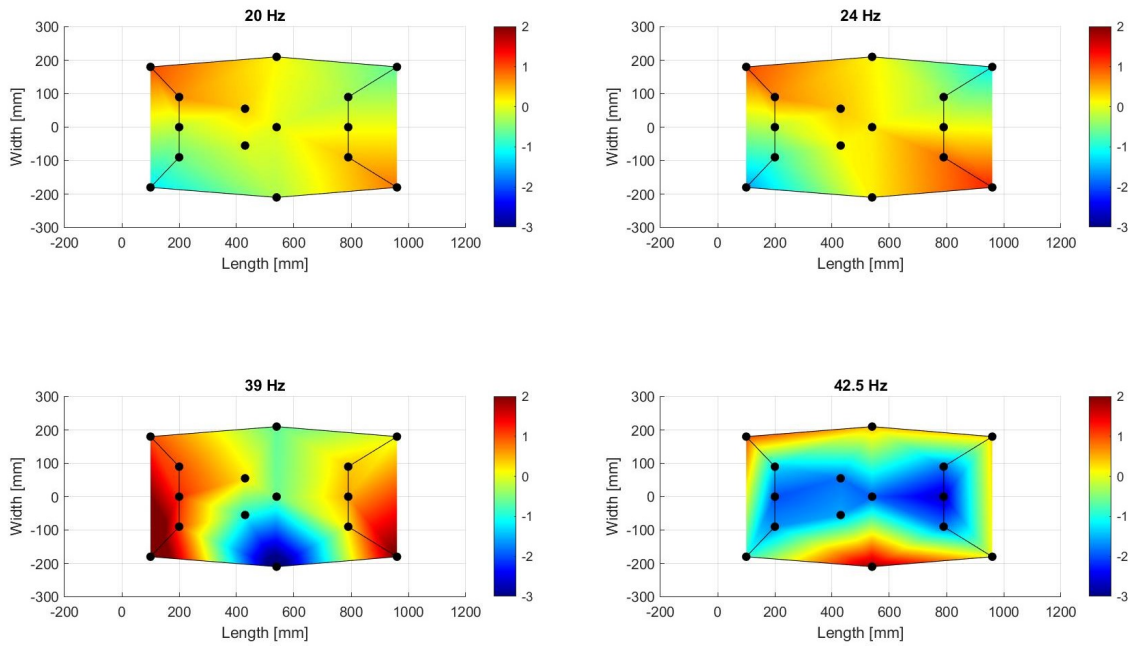
Figure 7.2: Mode shapes obtained from accelerometers tested in the water

These results will be further discussed in chapter 9, where they will be compared to the numerical predictions. The next section discusses the results of the accelerometers in air.

7.2 Accelerometers in air
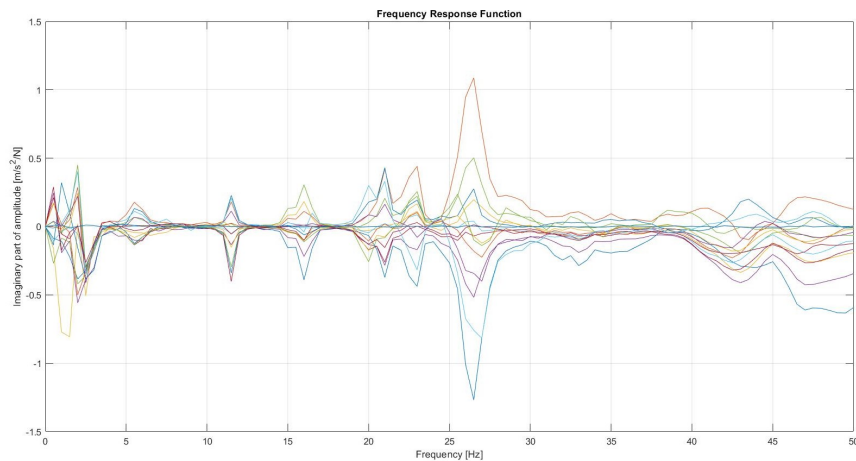
Figure 7.3: FRF of the dry configuration

Figure 7.3 depicts the frequency response spectrum of the dry configuration of the hammer tests. The figure shows that the following four frequencies can be identified, as the first four frequencies have mode shapes that show mostly global behaviour.

- 11.5 Hz
- 16 Hz
- 21 Hz

• 23 Hz
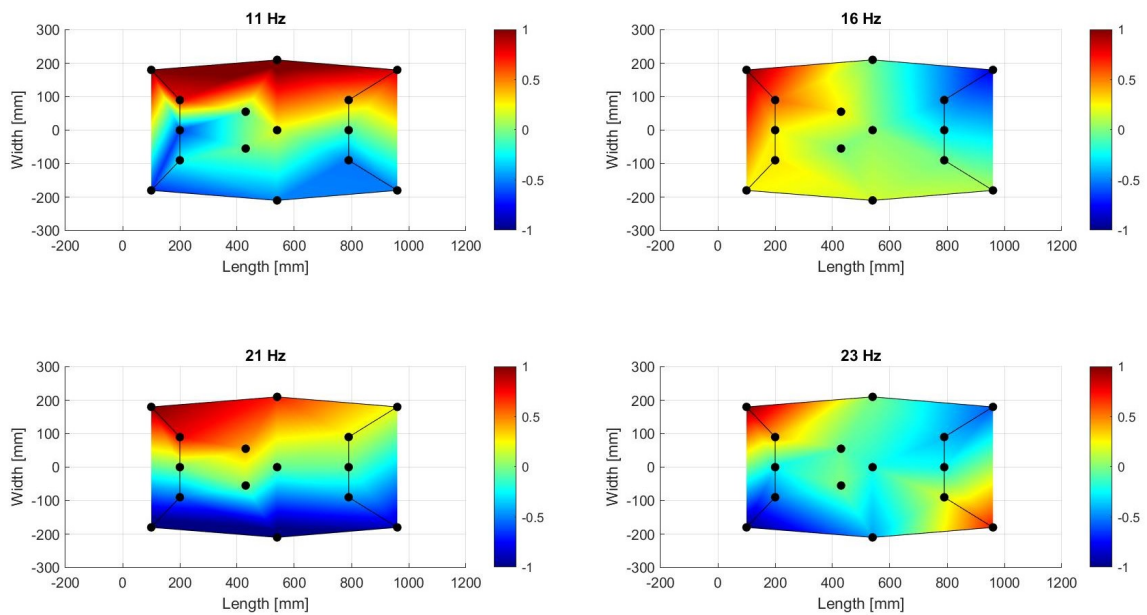
Figure 7.4: Mode shapes obtained from accelerometers, tested in air

Figure 7.4 depicts the mode shapes of the hammer tests performed in air. It can be seen that the mode shapes show primarily transverse deflections, which means that despite the low stiffness of the flexible supports (inner bicycle tube), the hammer impact on the model still significantly affected its structural response. The unexpected mode shapes can be introduced through the additional stiffness in the transverse direction.

7.3 DIC

The data is processed using the software: Istra4D. The images are imported, a mark and starting point are indicated, as well as setting the subset and grid space. It was decided to use a relatively large subset (facet size) and a small grid space, leading to a large overlap between sections. This led to the least amount of aliasing and to obtaining more global information. From Istra4D, the time and amplitude of the deformations in the z-direction with respect to the reference position are exported for every point within the mask.

As this led to a very large data set, 35 points were chosen for post-processing. Figure 7.5 shows the location of the points, both relative to the measured area (Figure 7.5b) and the location of the points compared to the measured surface area of the accelerometers (Figure 7.5a). The X-coordinates correspond to 580, 630, 680, 735, and 790 mm, and the Y-coordinates correspond to 90, 60, 30, 0, -30, -60 and -90 mm.
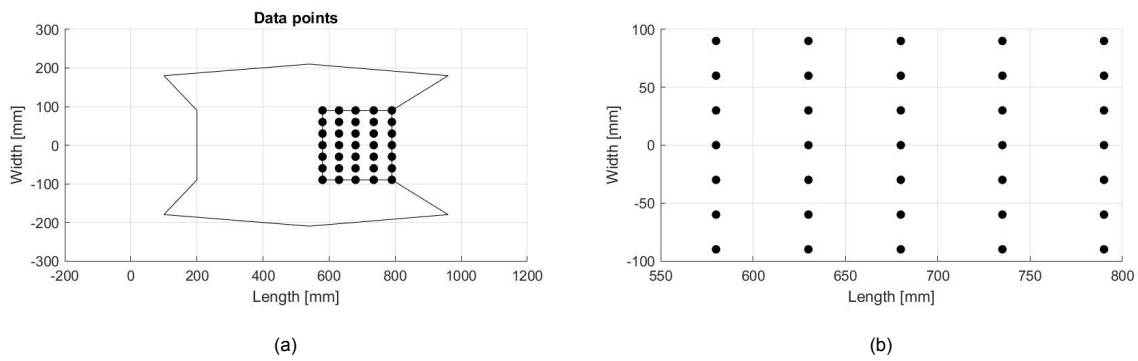
Figure 7.5: Location of the 35 data points of the DIC measurements. Subfigure (a) shows the points relative to the surface of the accelerometers and Subfigure (b) shows the area as obtained from the data.

Using the matlab function *fast fourier transform (FFT)* the data was transformed from the time domain to the frequency domain and again using the imaginary part of the amplitude to plot the FRF and mode shapes, which are again normalised. This led to the results discussed below.
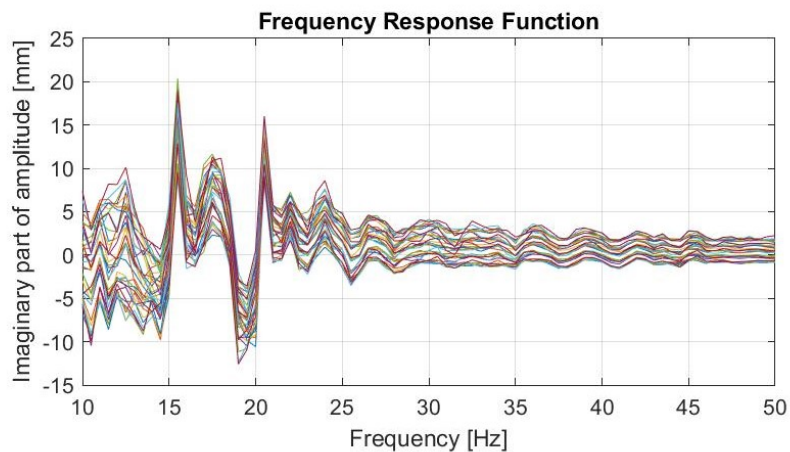
Figure 7.6: FRF of the DIC measurements.

Figure 7.6 depicts the FRF obtained with the DIC measurements, showing the resonance frequencies as listed below, and Figure 7.7 illustrates the corresponding mode shapes. From the graph, it can already be seen that the amplitude of the deformation is high, indicating unrealistic results.

- 15.5 Hz
- 17.5 Hz
- 19.5 Hz
- 20.5 Hz
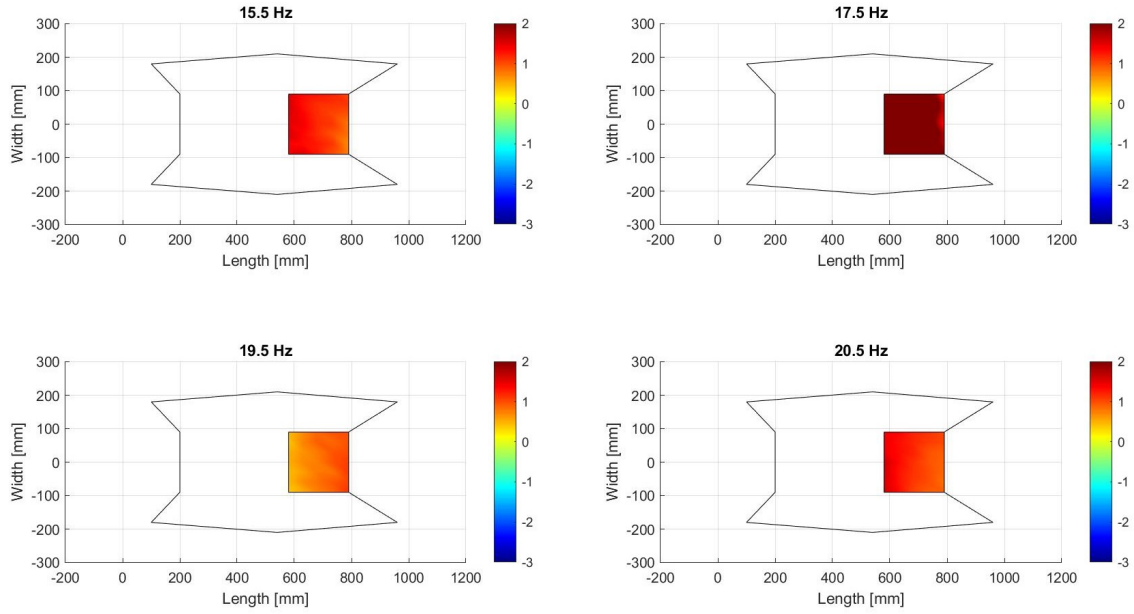
Figure 7.7: Mode shapes obtained with DIC measurements during hammer tests.

As the input for the hammer test in water was the same for both the accelerometers and the DIC, it can be expected that the resonance frequencies and mode shapes are the same, or at least similar. Figure 7.8 shows that the FRFs don't show the same resonance frequencies and that the amplitude of both graphs differs by an order of magnitude, also leading to different mode shapes. The exact difference in natural frequency can be found in Table 7.1.

(a)	(b)
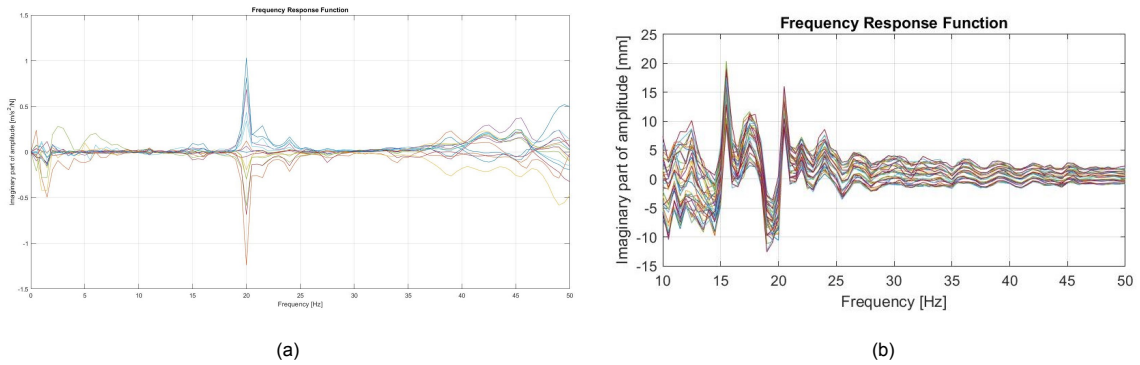
Figure 7.8: Comparison between the FRFs obtained with hammer tests in water. Subfigure (a) shows the FRF of the accelerometers and Subfigure (b) shows the FRF of the DIC.

Table 7.1: Comparison between the natural frequencies obtained with accelerometers and DIC

Accelerometer	DIC
20 Hz	15.5 Hz
24 Hz	17.5 Hz
39 Hz	19.5 Hz
42.5 Hz	20.5 Hz

It can be concluded that the DIC results don't give accurate results. This is most likely due to the application method of the speckle pattern. This application method is not preferred as it produces several

uncertainties: It is unknown whether or not the pattern properly adhered to the model, it is unknown if the paper/glue combination will follow the same deformations as the structure and it is unknown if the paper/glue combination attenuates the model's response.

More common application methods include spray painting speckles or free-handing speckles on the model. The latter is very time-consuming and the first option has been tried in this research, but it was found that the spray paint provided speckles that were too non-uniform. Thus, allocating time to find the right pattern, but more importantly, to find an appropriate application method is very important and should be taken into account in future research.

7.4 Conclusion

The inner bicycle tubes were used to minimise the disturbances in the structural responses of the model during the hammer impact. However, as mode shapes with an artificial character were observed, it can be concluded that the setup did affect the responses.
Furthermore, the DIC measurements didn't give reasonable results, however valuable lessons are learned for future research, emphasising the importance of the speckle pattern application method.

Overall, this chapter provides a detailed examination of the results obtained from the model experiments, highlighting the presence of resonance frequencies, from which the first four natural frequencies are identified, and the mode shapes of the model experiments. The modal properties obtained from the accelerometers in water will be compared to numerical predictions after they are obtained in the next chapter.

8
Numerical analysis

To compare the modal properties of the model experiments, numerical analysis has to be performed. To gain insight into the effects certain design and numerical modelling decisions have had on the natural properties, including modelling the point masses, analyses are performed for the fully elastic model, the full-scale model, and the production model.

8.1 Full-scale model

This section explains how the full-scale model is analysed numerically. The input used to numerically model the full-scale model is the following:

- Steel
- Uniform thickness of 73 mm
- Crane and cargo modelled as point masses that behave deformable
- Mesh size of 1.5 m
- Mass distribution:

Table 8.1: Mass distribution used as input for the full-scale model.

Description	Weight [ton]	LCG [m]	TCG [m]	VCG [m]
Structure	67442	96	0	14
Crane	7220	97	-31	65
Cargo	10000	96	0	25

Figure 8.1 displays the first four mode shapes of the full-scale model and shows that they exhibit mainly global behaviour. The natural frequencies that accompany these mode shapes are:

- 1.322 Hz
- 1.494 Hz
- 2.475 Hz
- 2.600 Hz
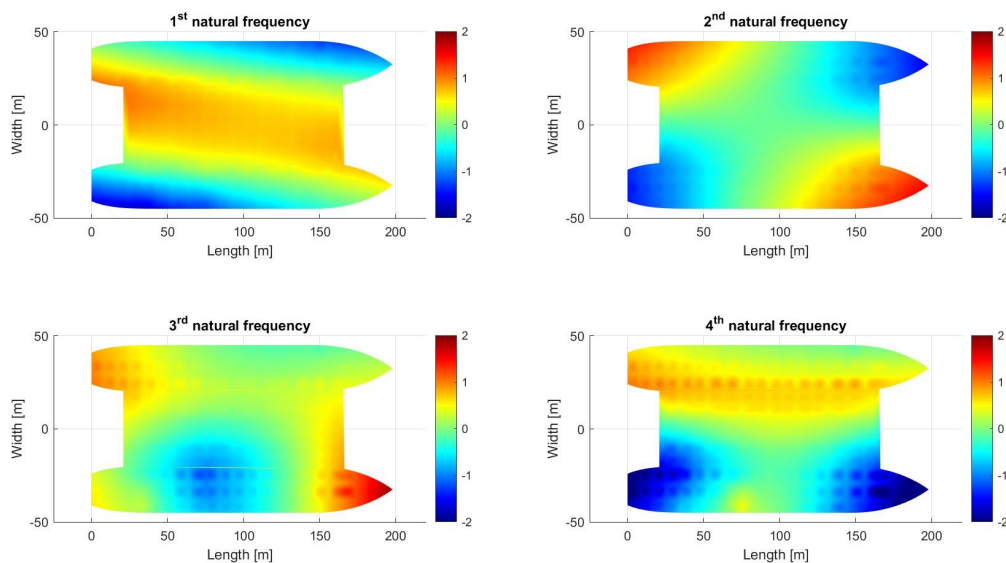
Figure 8.1: First four mode shapes of the full-scale model.

The figure illustrates that mode shapes 1,2 and 4 correspond to deformations of the cross-deck, whereas the third one is the 2-node bending mode of the hulls. The reason only one of the hulls is deforming is due to a slight mass asymmetry.

8.2 Production model

The input for the numerical production model is
- PETG
- Mesh size of 5 mm
- Uniform thickness of 0.56 mm
- Lead block distribution as depicted in Table 3.4
- Cargo and crane modelled as point masses with a deformable behaviour
- The following mass distribution:

Table 8.2: Mass distribution used as input for the production model.

Description	Weight [kg]	LCG [mm]	TCG [mm]	VCG [mm]
PETG structure	2.4	532	0	80
Lead blocks	8.75	545	-1	56
Crane	1.24	539	-172	450
Cargo	1.71	528	128	394
Total	14.1	540	0	136

This leads to the natural frequencies below and the mode shapes as depicted in Figure 8.2.
- 19.165 Hz
- 23.127 Hz
- 36.448 Hz
- 38.813 Hz
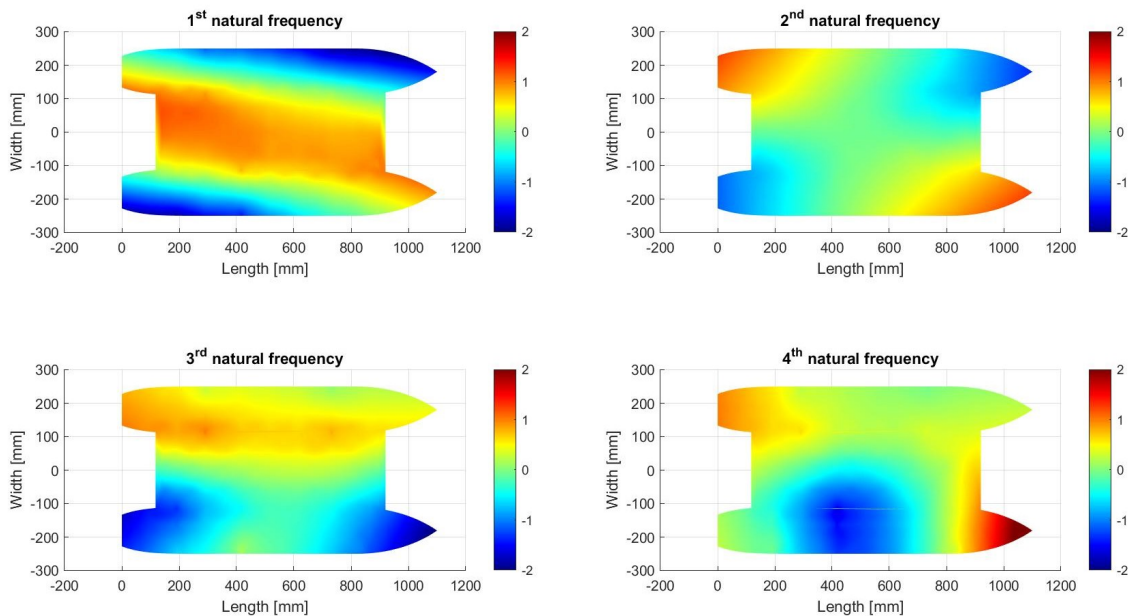
Figure 8.2: First four mode shapes of the designed model using rigid point masses.

8.3 Fully elastic model

As changes had to be made during the production process, differences can be found between the production model and the elastic model. To compare the modal properties of the structure to the numerical predictions, the numerical model must have the same input as the elastic model, see the list below:

- PETG
- Crane and cargo
  - Modelled as point masses that behave rigidly
  - Including inertia and mass distribution of support structures
- Updated thicknesses
  - Longitudinal plates: 0.58 mm
  - Bulkheads: 0.58 mm
  - Web frames: 0.52 mm
- Lead blocks, all modelled as rigid point masses
  - 35 lead blocks inside of the hull, according to Table 3.4
  - 2 extra lead blocks on the cross-deck
- Mass distribution:

Table 8.3: Mass distribution as input for the fully elastic model.

Description	Weight [kg]	LCG [mm]	TCG [mm]	VCG [mm]
Structure	2.4	533	0	80
Lead blocks	9.3	555	-3	61
Crane	1.4	445	-173	327
Cargo	2.0	535	136	369
Total	15.1	543	0.3	131

These modifications lead to the natural frequencies listed below and the mode shapes as shown in Figure 8.3

- 21.654 Hz
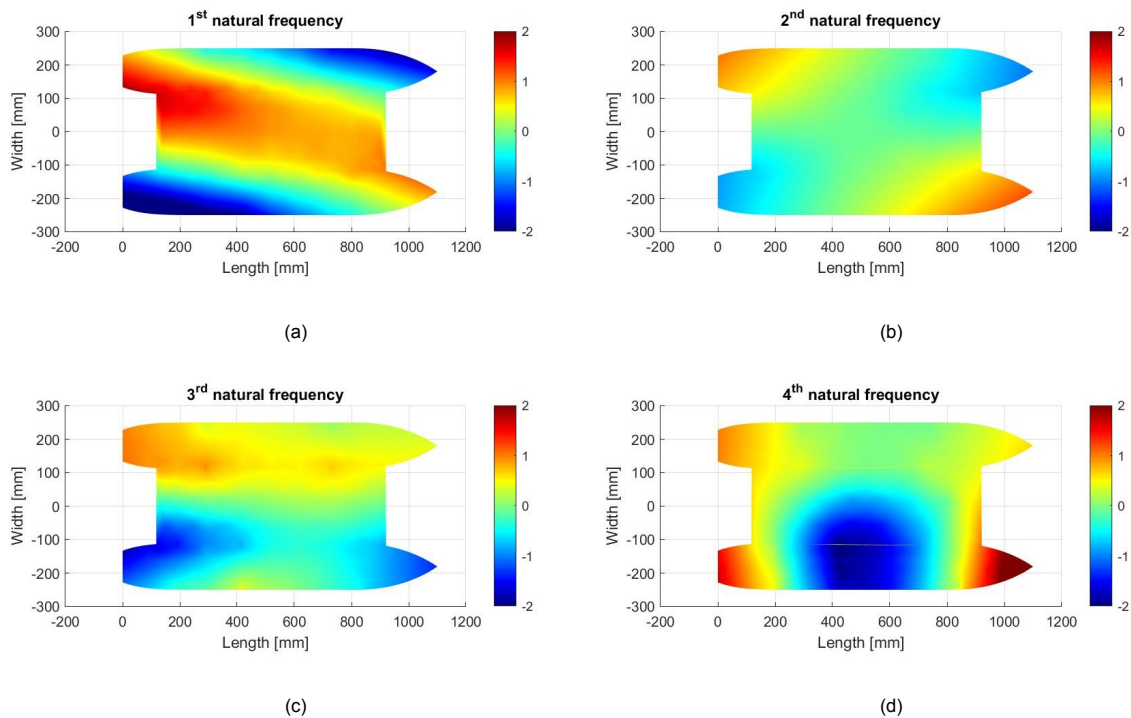- 23.690 Hz
- 39.863 Hz
- 44.135 Hz

(a)

(b)

(c)

(d)

Figure 8.3: First four mode shapes of the produced model.

8.4 Behaviour of point masses

As listed in the input of both the full-scale model and the production model, the point masses are modelled to behave as deformable point masses, while the point masses of the fully elastic model are modelled to behave rigidly. To compare the numerical results to the results of the model experiments, the numerical model has to represent the physical model as accurately as possible. Therefore, the behaviour of the point masses had to be changed from deformable to rigid: Because 1) for the support structures of the crane and the cargo, the rigid behaviour is a closer resemblance, as they are designed to be rigid (section 8.2), and 2) for the lead blocks, this also has to do with the behaviour of the surfaces to which the point masses are connected to as the lead blocks cover almost the whole plate, and are themselves rigid, seeing the lead won't deform under the exerted pressure, therefore, the plates to which they are attached to, will behave rigidly as well.

The natural properties of the fully elastic model, when still using the deformable point masses, would lead to the natural frequencies in the list below and the mode shapes depicted by Figure 8.4.
- 19.284
- 20.584
- 32.911
- 34.462
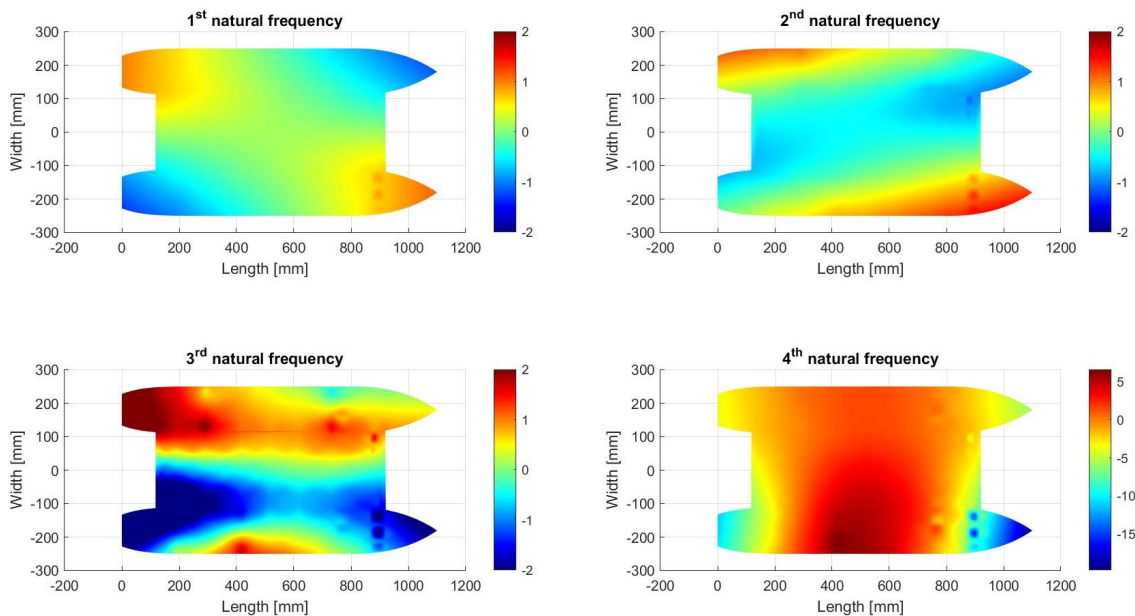
Figure 8.4: The first four mode shapes of the fully elastic model, using deformable point masses.

Table 8.5 lists both the natural properties of the fully elastic model when point masses are modelled to behave both deformable, as well as rigid. It can be seen that the natural frequencies of the rigid point masses are higher than those of the deformable point masses, this can also be seen by the extent to which both models deform. Both locally and globally, the mode shapes with deformable point masses show more extreme responses. Locally, this can be seen from the fact that the position of the lead block on the starboard side hull can be easily seen due to local responses, and globally, it can be seen that, especially, the 3rd and 4th mode shape, show higher deflections.

Both the full-scale model and the production model are modelled with deformable point masses, and thus decisions were made based on their natural properties. Table 8.4 shows the full-scale frequency, the target frequency, the production frequency, and lastly, the fully elastic frequency for both point mass behaviours. It can be seen that both behaviours have different natural frequencies and that the natural frequencies of the rigid point masses show more deviation from the calculated target frequency than

the deformable point masses. This is because the natural frequencies of the production model were obtained by moving around the lead blocks until the frequency matched up with the target frequency, which was calculated by scaling down the frequencies of the full-scale model with deformable point masses. When rigid point masses were used, not only for the fully elastic model but also for the two other models, it is expected that the fully elastic model using rigid point masses would represent the target values for the natural frequency better. However, it is difficult to make a statement on how much the placement of the lead blocks influences the natural frequency of the fully elastic model.

Deformable point masses				Rigid point masses			
Full-scale	Target	Production	Fully elastic	Full-scale	Target	Production	Fully elastic
1.322	17.736	17.791	19.284	1.383	18.555	19.165	21.645
1.494	20.044	19.894	20.584	1.967	22.768	23.127	23.690
2.475	33.206	30.662	32.911	2.694	36.144	36.448	39.863
2.600	34.883	32.533	34.462	2.791	37.445	38.813	44.135

Table 8.4: Natural frequencies full-scale model, target (calculated), produced model, and fully elastic model for both deformable point masses and rigid point masses.

Table 8.5: Comparison between modelling point masses as deformable or rigid for the fully elastic model.

Mode shapes		Frequency	
Deformable	Rigid	Deform.	Rigid
		19.284	21.645
		20.584	23.690
		32.911	39.863
		34.462	44.135
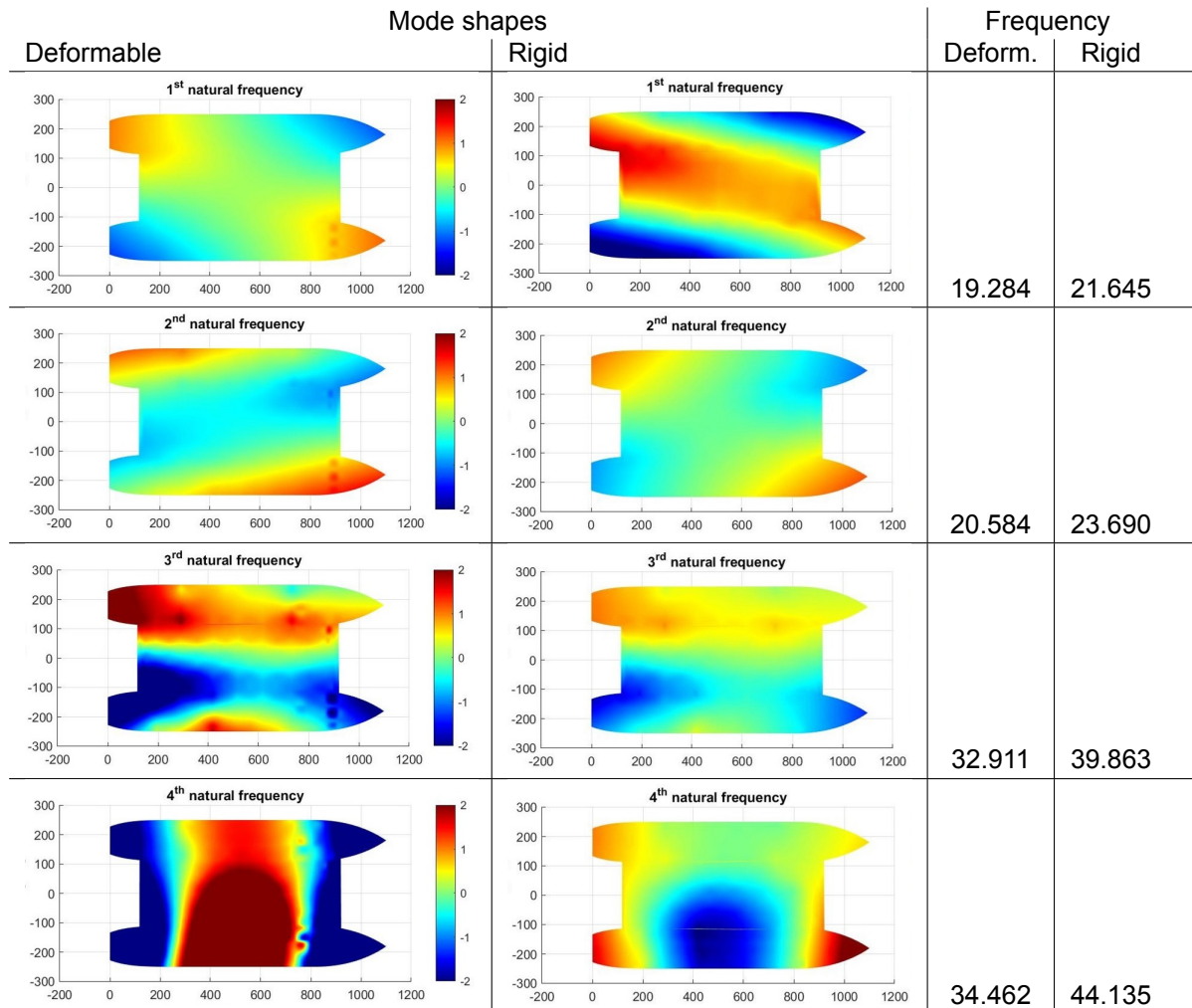
8.5 Conclusion

From this chapter, it can be concluded that the behaviour of the point masses influences the natural properties of a model, however, how significant this influence is, can't be commented on. Additionally, when looking at the mode shapes of the full-scale model and those of the production model, it can be concluded that the lead blocks don't have a significant influence on the mode shapes, as both models show similar deformation patterns. Furthermore, the natural properties, obtained by numerical analysis of the fully elastic model using rigid point masses, have to be used to compare to the modal properties obtained by model experiments.

9

Comparison

This chapter will compare the identified modal properties of the fully elastic model to the numerical predictions. More specifically, the modal properties, acquired during the hammer test in water, using accelerometers, are compared to the numerically obtained modal properties, obtained by performing modal analysis in air, using the fully elastic model, where the point masses are modelled to behave rigidly.
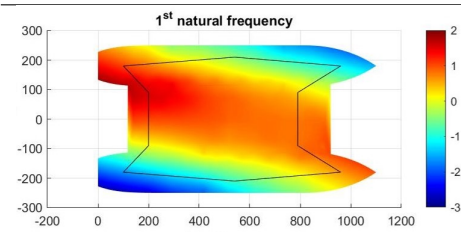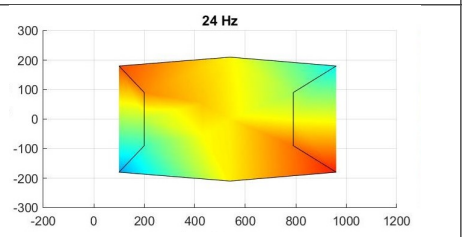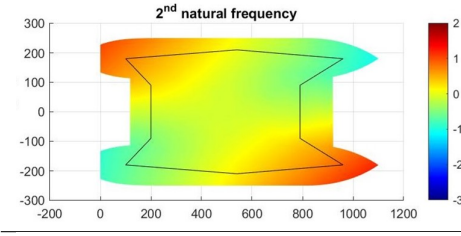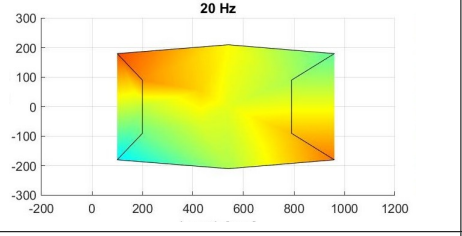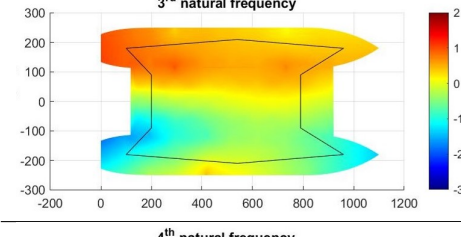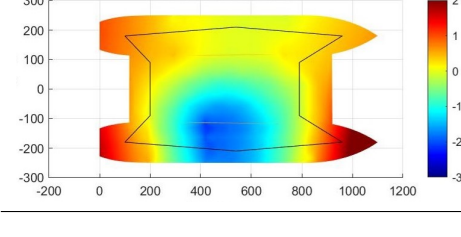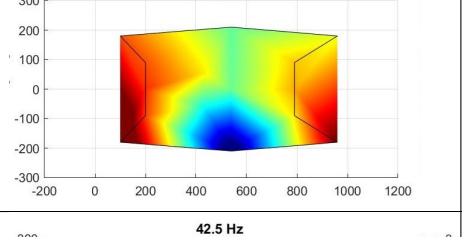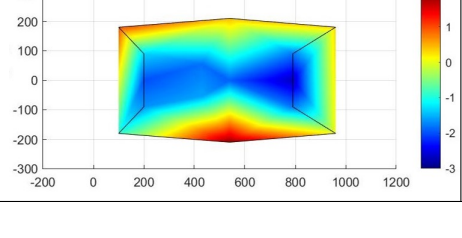
Table 9.1 shows per row, the similar mode shapes, if they exist, followed by the corresponding natural frequencies. It can be seen that the 1st, 2nd and 4th numerical mode shapes could be matched to the 2nd, 1st and 3rd experimental mode shapes. It could be concluded that there is a difference in the order of the mode shapes, however, from performing many different numerical simulations, it was demonstrated that, for such complex structures with mode shapes combining several directions of response, even a slight change in mass distribution can significantly affect the mode shapes. Even, though more or less the same mode shapes were always present, the order of the mode shapes was inconsistent. Furthermore, the 3rd numerical mode shape doesn't show any similarity to the 4th experimental mode shape.

The observed differences between the numerical analysis of the fully elastic model in air and the experimental model in water can be attributed to several factors.

One known difference is the presence of epoxy in the experimental model, which likely adds stiffness to the structure. However, the extent to which it influences the results is uncertain. Additionally, the magnitude of the added mass effect in water, depending on the displacement of fluid by the model, can lead to differences. To better understand and predict the effect of the magnitude of the added mass, hydrodynamic simulations should be performed.

Differences in the precise distribution of mass, if present, within the model can influence the mode shapes and natural frequencies. Likewise, variations in transverse thicknesses, including those of the bulkheads and web frames, could contribute to the differences in the natural properties as well, however, it is unsure if these variations are indeed present. Longitudinal thicknesses, however, are known to be consistent between both models and thus are not a source of differences in the natural properties. Similarly, the mass of the PETG used for the structure of the experimental model is not a factor contributing to the observed differences, as it is extensively measured and the deviations are known.

Table 9.1: Comparison between numerically obtained data for the fully elastic model and the accelerometers in water.

Mode shapes		Frequency	
Numerical	In water	Numerical	Water
		19.165	24
		23.127	20
		36.448	
		38.813	39
			42.5

10
Conclusion

The current research aimed to investigate the design and production of a fully elastic model of a catamaran for hydroelastic experiments.

The objectives used to reach the aim were as follows:

1. Design a globally scaled model of a catamaran, including all primary members of the hull structure.
2. Produce the model out of polymer using additive manufacturing.
3. Plan and install instrumentation capable of capturing longitudinal and transverse responses.
4. Identify the modal properties of the structure and compare them to the numerical predictions.

Designing the fully elastic model was done in three steps: 1) Introducing the reference vessel and using its structure and mass distribution to obtain the full-scale model. 2) Selecting a scaling factor and scaling the full-scale model, and 3). Designing a model that can be produced using additive manufacturing. The design method showed good agreement between the full-scale model and the production model, and by observing their mode shapes, the concern that the lead blocks, added to the internal structure of the model, impact the response of the model was mitigated.

Production of the fully elastic model consisted of 3D printing the production model out of PETG, with a two-perimeter thickness, and assembling the sections using epoxy. The additive manufacturing method proved to be successful in obtaining a fully elastic model used for hydroelastic experiments, but it also provided challenges regarding the single-perimeter surfaces.

Verification of the fully elastic model was done by comparing the modal properties to numerical predictions.
Model experiments were performed in water and air with both accelerometers and DIC measurements. The model experiments illustrate that the setup, using accelerometers, in water, shows reliable results, but it also raises questions regarding the setup in air and the setup of DIC. The results for the experiments in air showed artificial mode shapes, additionally, as the mode shapes in water did present mode shapes similar to the numerical predictions, it can be concluded with high certainty that the problem is with the setup in air and not with the model.

Furthermore, it was found that the setup in the flume tank used to obtain the DIC measurements needed changes regarding the camera setup, as the cross-deck is now only partly inside of the view of the cameras. Furthermore, the results of the data that was obtained, show unrealistic deformations and thus mode shapes, which are caused by the application of the speckle pattern.

Numerical experiments were performed to determine the influence of the behaviour of the point masses and it was found that rigid point masses have to be used.

Comparison between the modal properties of the fully elastic model against the numerical prediction, showed mode shapes that agreed well with one another, however as the magnitude of the added mass is unknown, it is uncertain how much value the comparison holds. To accurately compare the results, hydrodynamic simulations should be compared.

In conclusion. this research has shown that by using additive manufacturing, a flexible model can be produced, that allows mode shapes of the cross-deck to be excited in all directions.

11
Recommended research

The current research leaves a potential for further research. The recommended research is broken down into three categories: modal experiments, hydrodynamic experiments, and hydroelastic experiments.

Modal experiments

- Developing a support system for testing in air that does not cause interference with the model.

- Calculating the mode shapes in water and their corresponding mode shapes.

- Perform modal tests using a shaker, as some of the more dominant modes tend to mask the others in the frequency response during hammer testing.

Verify the hydrodynamic behaviour of the model

- Determine the exact COM using a pendulum test.

- Perform model experiments using motion-tracking to obtain the RAO's of the model

- Compare the hydrodynamic behaviour of the model against AQWA simulations.

Hydroelastic cross-deck slamming investigations

- Using pressure sensors to measure the water impact on the cross-deck

- Developing an application method for the speckle patterns needed for DIC experiments.

- Obtaining the cross-deck deformations from the high-speed cameras using DIC.

A
Detailed mass distribution

Table A.1: Detailed mass distribution of the reference vessel.

	Description	Weight [ton]	LCG [m]	TCG [m]	VCG [m]
Light weight	Steel hull preservation	36536	95	3	15
	Ship's equipment	320	132	14	22
	Accommodation and service spaces	443	170	26	32
	Electrical and nautical installation	745	109	11	15
	Main and aux. Propulsion equipment	1000	92	15	12
	Auxiliaries and piping inside engine room	800	126	18	21
	Auxiliaries and piping outside engine room	400	109	3	13
Deadweight	Anti heeling tanks	12339	83	-27	18
	Water ballast	9148	125	9	5
	Fuel oil	2352	109	27	6
	Fresh water	370	155	21	9
	Displacement losses	985	98	0	3
	Misc tank fillings	250	99	0	23
	Crew and effects	10	99	0	23
	Spares and Stores	50	99	0	23
	Crane	7220	97	31	65
	Main deck cargo	10000	95	-23	71
	Total	84604	98	0	25

B
Construction drawings

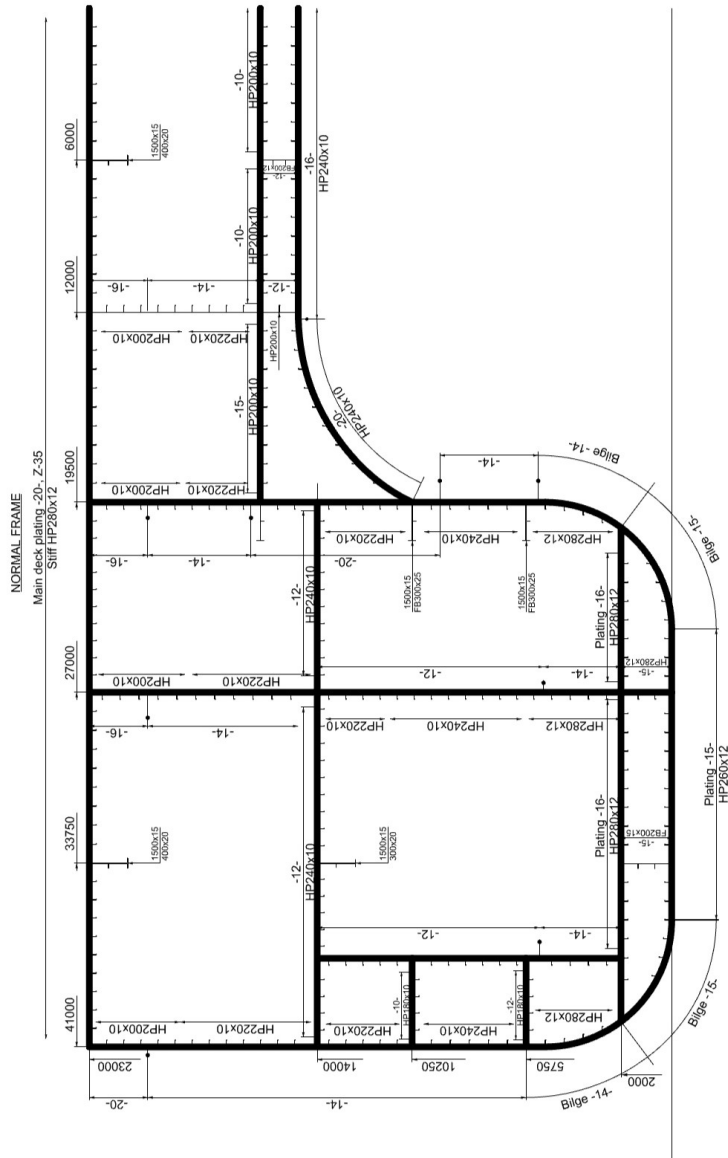Figure B.1: Construction drawing of the reference vessel
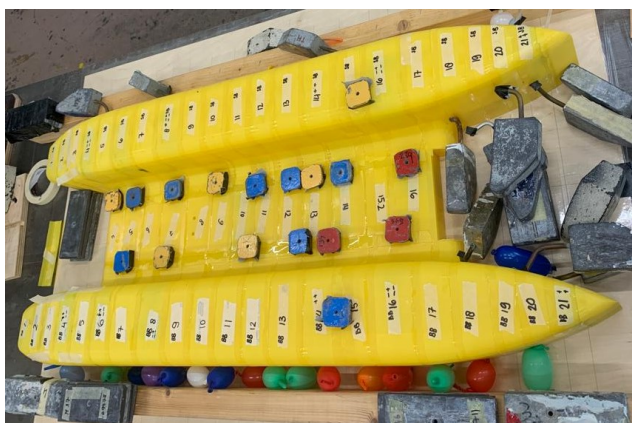
Assembling the model

Figure C.1: Measures to limit buckling during the joining of the sections
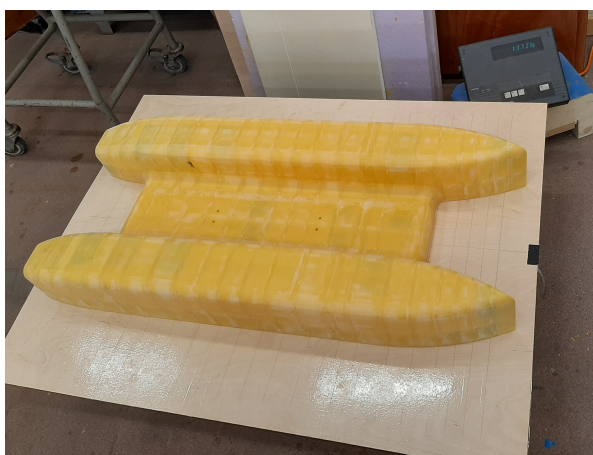

Figure C.2: First weigh in before epoxy

Figure C.3: Model after the final layer of epoxy

Figure C.4: Adding the waterline to the model

Figure C.5: Final weigh-in of the model including all add-ons

D

Paper writen for the HSMV conference

The design, production, verification, and calibration of an elastic model of a catamaran for hydroelastic experiments

Anabel KESER [a], Michiel VERDULT [b] Harleigh SEYFFERT [a] and
Apostolos GRAMMATIKOPOULOS [a,1]

[a] *Maritime and Transport Technology, Delft University of Technology, Delft, The Netherlands*
[b] *Vuyk Engineering, Rotterdam, The Netherlands*
ORCiD ID: Apostolos Grammatikopoulos https://orcid.org/0000-0003-1800-7406

Abstract. Catamarans are popular in the offshore sector as they combine good transverse stability and ample deck space with low wave resistance. However, their slender hull shape results in low restoring qualities in heave and pitch motions. The large motions in rough weather can often result in water impacting the underside of the deck connecting the two hulls, a phenomenon called wet deck slamming. The impulse excitation from wet deck slamming can then produce a transient hydroelastic response of the structure called whipping. Whipping excites mode shapes that would not normally be present in the response, as their natural frequencies are significantly higher than the wave encounter frequency. This results in detrimental contributions to fatigue life through high-amplitude cyclical bending moments. Both the calculation of slamming loads and the prediction of resulting structural responses have been a challenge for several decades. The highly nonlinear and three-dimensional character of the phenomenon, combined with the strongly coupled fluid-structure interaction means that it is unpredictable, and even the definition of slamming events has been a matter of disagreement among researchers. Experiments are still a vital part of these investigations, for validating ever-improving numerical techniques. An essential issue with experiments is the extent to which mode shapes and natural frequencies can be emulated in model scale. Traditional hydroelastic models are segmented and use either a flexible backbone or flexible joints to introduce stiffness. This often results in an excellent description of the 2-node bending mode, but an increasing error for higher modes leads to stress inaccuracies. In this investigation, a continuous model of a catamaran is designed and produced for hydroelastic experiments. The advantages and limitations of the concept are identified, the verification against structural models is presented, and the calibration of the measurements is discussed.

Keywords. additive manufacturing, elastic model, hydroelasticity, scaling, slamming, whipping

---

[1]Corresponding Author: Apostolos Grammatikopoulos, A.Grammatikopoulos@tudelft.nl

1. Introduction

Scaling the hydroelastic response of ships requires a mass distribution, bending stiffness, and natural frequencies which are representative of the full-scale vessel [1]. Hydroelastic experiments for ships are usually performed with so-called segmented models. For these models, the bending stiffness is introduced using either a flexible backbone [2] or flexible joints [3], which link the segments together. By choosing the correct stiffness, the first symmetric natural frequency can be emulated. The way a segmented model is designed and manufactured allows relative flexibility of material properties and sizing, but it is challenging to scale higher natural frequencies, which causes inaccuracies in strain scaling.

Although elastic models are almost as old as ship hydroelastic experiments in general (e.g., [4,5]), their presence in the literature is relatively limited [6]. The disadvantages of a continuous model are mainly related to the difficulties associated with its design and production. The scaling of the plating and stiffeners can lead to very small thickness and, once the scaling has been performed successfully, manufacturing the model can be time-consuming and expensive. Consequently, there have been hardly any elastic models in the past twenty years - one exception being the work by Houtani et al., who manufactured their model using polyurethane foam [7]. New opportunities appeared with the advancement of additive manufacturing techniques. 3D modal testing, together with FEM proved capable of predicting the natural frequencies of complex thin-walled structures [8]. With this method, the first continuous model that closely resembled the detailed internal structure of a monohull (the so-called fully-elastic model) was designed, produced, and tested. It was demonstrated that both global and local responses can be measured and that the model can accurately emulate the mode shapes and natural frequencies [9].

However, this model still had an almost beam-like behaviour, which is not true for catamarans. The wet deck is often significantly more flexible than the hulls, meaning that the transverse mode shapes can have natural frequencies which are lower than the longitudinal ones. Traditional segmented models are unable to capture these transverse responses, but even elastic models have not been used in this manner.

In this investigation, additive manufacturing is used to produce a fully-elastic model of a catamaran. The ultimate purpose is to use this model for hydroelastic experiments to measure the transient structural dynamic responses (whipping) under slamming excitation. This paper, however, is focusing on the steps before the wet testing. The design procedure is described, the advantages and limitations of the concept are identified and the calibration of the measurements is discussed.

2. Model design

2.1. *Full-scale analysis*

The full-scale ship is based on a reference catamaran provided by Vuyk engineering. The dimensions of this vessel can be found in Table 1. The reference vessel had to be modified for two main reasons. Firstly, the structural detail had to be reduced slightly (for instance, by not including local stiffeners) while allowing the first four mode shapes

Table 1. Principal particulars of the full-scale ship and the 1/180 scaled model.

Dimension	Full scale	Model scale
L (Length)	198 m	1100 mm
B (Beam)	90 m	500 mm
D (Depth)	26 m	144.4 mm
T (Draft)	10.5 m	58.3 mm
Δ (Displacement)	84603.5 ton	14.51 kg

to primarily exhibit global behaviour. Secondly, the model had to be adjusted to facilitate easy scalability.

The bulkheads and 'main' longitudinal internal structure were used, with the thicknesses of the reference vessel as the starting point and structural elements were added accordingly. This first combination did not produce any global mode shapes. The equivalent thicknesses were then calculated instead, stiffening the local structure without adding all the geometric detail, to make the first mode shape a global one. Adding girders and stringers to the structure provided a second global mode shape. Web frames were added in between each pair of bulkheads, which led to a third global mode shape. Lastly, the fourth mode shape was obtained by adding the mass of the deck cargo and crane to the modal analysis, which affected the global natural frequencies more significantly than the local ones. The final mode shapes can be found in Figure 1. The first three mode shapes correspond to deformations of the wet deck, whereas the fourth one is the 2-node bending mode of the hulls. The reason only one of the hulls is deforming is due to a slight mass asymmetry.
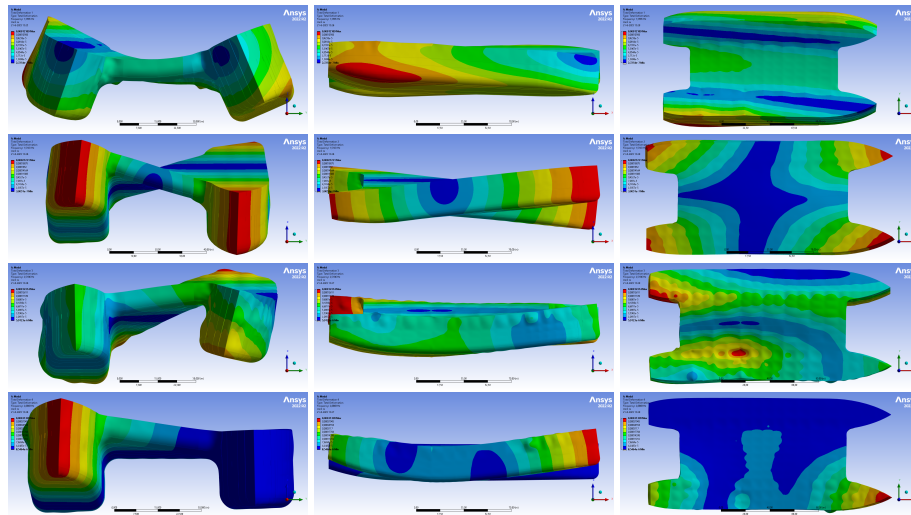

Figure 1. First four mode shapes of the full scale model. Each row corresponds to a mode shape, and the three columns correspond to front view, side view, and top view, respectively.

2.2. Scaling

The scaling factor depends on various restrictions and limitations, which are categorized into two groups: dimensional requirements and compatibility for experiments. In terms

of dimensions, the model must fit within the flume tank where experiments are planned, and the 3D printer should be able to produce the minimum wall thickness. For the experiments, it is important that the wavelengths between 1/2 to 2 times the length of the ship are tested, and the forward speed is up to 2.5 m/s (maximum forward speed for the flume tank).

Ideally, the Young's modulus (E) of the material should scale linearly with the scaling factor λ, and the second moment of area (I) of the cross section with λ^4. This would mean that all thicknesses would also scale linearly, which was impossible due to the minimum printable thickness. Consequently, it was decided that EI will be scaled as a whole with λ^5. This meant that there was room to use the low material stiffness to design with higher thicknesses (more scaling down absorbed by the material side than the thickness side).

Based on the size of the flume tank, the range of potential scaling factors was determined to be between 90 and 180. This range was then examined against minimum printable thickness, which was determined as the one corresponding to two perimeters (in this case 0.56 mm). Modal analysis was performed for the different scaling factors, with the goal of obtaining four global mode shapes, without going below this minimum thickness. The first attempt indicated a scaling factor of $\lambda = 130$, with thicknesses of $t = 0.7$, 0.8, 1.0, and 1.6 mm as the optimal choice. In order to simplify manufacturing, it was decided to use a uniform thickness of 0.84 mm, corresponding to 3 perimeters, which achieved a second moment of area very close to the original section with the non-uniform thickness. Although $\lambda = 130$ was viable from a structural perspective, the longest waves that could be generated in the flume would barely reach the ship-wave matching region. Consequently, it was decided to use a scaling factor $\lambda = 180$ instead. This significantly reduced the expected printing time as well, and necessitated fewer splits along the breadth of the vessel to fit in the printer. The only concern was the structural strength of the new thickness of 0.56 mm (corresponding to two perimeters). Initial test prints confirmed that 0.56 mm was a viable option.

Of course, the flexural modulus is not the only material difference between full scale and model scale, as the density also changes. As the density of PETG is much lower than the density of steel, the model is much lighter after scaling than its required mass. Therefore, ballast masses have to be added throughout the model so that both the mass, centre of gravity and natural frequencies agree with the target scaled values (multiplied from full-scale by $\sqrt{\lambda}$). Figure 2 contains the distribution of the masses added to the model, which leads to the natural frequencies obtained from ANSYS that can be seen in Table 2. Good agreement between the two was achieved.
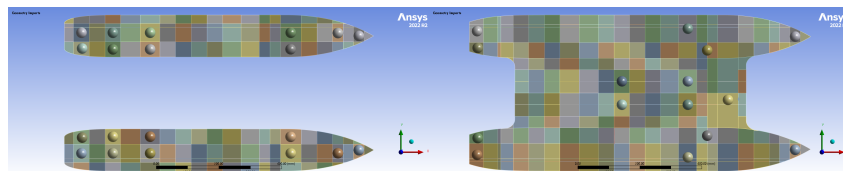

Figure 2. The distribution of added lead masses. The left figure shows the masses on the bottom deck and the right picture shows the masses at the middle deck and wet deck.

Table 2. Natural frequencies full-scale model, scaled model (calculated) and scaled model from ANSYS

Mode shape	Full scale frequency [Hz]	Target scaled frequency [Hz]	ANSYS frequency [Hz]
1	1.329	17.826	17.792
2	1.492	20.017	20.763
3	2.489	33.392	33.072
4	2.687	35.050	35.104

2.3. Design for 3D printing

Following scaling of the model structure, the main concerns regarded its manufacturing and the necessity to make it watertight. As the printer dimensions are 24 cm by 20 cm by 20 cm, the model had to be split up into multiple segments to be assembled after printing. The vessel was split in transverse direction in three parts, namely the wet deck and the two hulls. Originally, the longitudinal division was supposed to be at every bulkhead. In that case, the web frame along with the longitudinals attached to it was going to be printed separately from the main section, which would be printed from the bulkhead up, see Figure 3a and Figure 3b, to almost eliminate the need for support material. The web frame would sit partly on the longitudinals of the main section and partly on a protruding perimeter. However, a test print revealed that not only the support for the web frame was insufficient, resulting in insecure attachment, but also the lack of supporting structure inside the main section resulted in severe buckling of the plating (Figure 4). It was decided to split the model at both the bulkheads and the web frames instead, and include all structure for the entire length of these sections. (Figure 3c and Figure 3d).

(a)   (b)

(c)   (d)
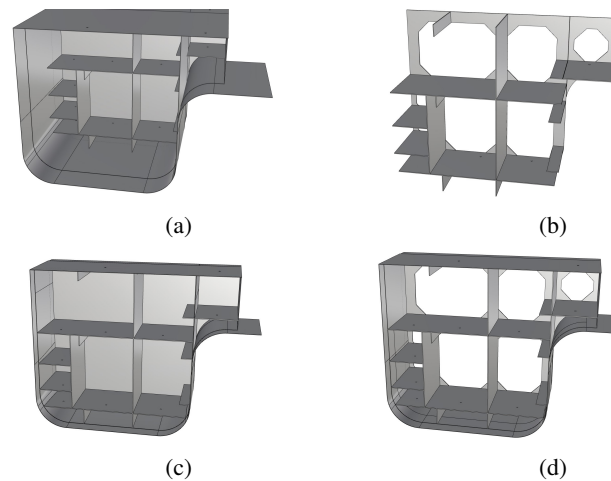
Figure 3. Longitudinal division of the model. Subfigures (a) and (b) depict the original design and the Subfigures (c) and (d) depict the revised and final design.

Then the segments were designed to be assembled with an overlapping system: The whole model was printed with a double perimeter (0.56 mm). At each section, there was 1 cm, at both ends (front and back), where only one perimeter would be printed. In the front this is the outer perimeter and the back it is the inner perimeters, which means that,

Figure 4. Buckling of the overlap section

in theory, two successive sections slide together perfectly and can then be glued together using a thin layer of epoxy, which will also ensure no water leaking through.

The length of the overlap is not completely arbitrary. Before using an overlap length of a centimetre, a quarter of the length of a segment was used instead. However, this accentuat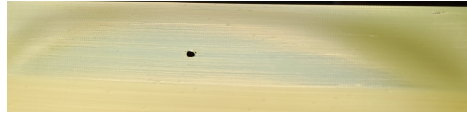ed the buckling issues described previously. Figure 4 depicts buckling of such an overlap section - it should be emphasised that the hole in the middle is not a result of failure, but one of the drainage holes mentioned earlier, which is slightly malformed because of the buckling.

3. Model production

All structures were produced using the same printer, material, and set of parameters. A Prusa i3 MK3 printer was used, which was modified with a Bondtech extruder and an E3D 0.25 mm brass nozzle. The material used was eSUN PETG, which was maintained dry by being stored in an eSUN eBox Lite at a temperature of 50° C. During printing, the nozzle temperature was 230° C and the bed temperature was 80° C. The height of the first layer was 0.15 mm, and 0.125 mm for all other layers, whereas the extrusion width was set at 0.28 mm. All longitudinal components were printed using only perimeters, of which the external ones were printed at a speed of 35 mm/s, and the internal ones were printed at a speed of 65 mm/s. The bulkheads and web frames were printed with 100% rectilinear infill, at a speed of 30 mm/s.

All structures were printed with the longitudinal axis of the ship coinciding the vertical axis of printing (layering direction). This decision was made as ships have a nearly prismatic geometry along the length, which can be printed very efficiently vertically. Since the vessel was split at each bulkhead and each web frame, these parts of the structure were printed first on the build plate, ensuring sufficient adhesion. Subsequently, the remainder of the section was printed with little to no need for support material.

Due to the small intended thickness, most of the longitudinal components of the model were printed with two perimeters of material, for an intended thickness of approximately 0.6 mm. At the locations where sections would be joined together, a single perimeter thickness was used, as the thickness was split between the two neighbouring sections to create an overlap at the joint. This meant that the first and last cm of each section only had a single perimeter. Similarly, the innermost parts of the hulls, where they would be connected to the wet deck sections, also had a single-perimeter thickness. Unsurprisingly, these proved to be the areas of the structure featuring the most production issues. These included:

1. Spots of "missing" material near the end of the sections close to the bulkhead or web frame. These were generated in areas where the printer started generating a perimeter at the location of a deck or stiffener (Figure 5a).

(a)   (b)

Figure 5. Common issues in areas of single-perimeter thickness: (a) Missing material near stiffeners (left); poor printing of overhanging walls (right) (b) Separation of side wall from bulkhead due to plate buckling.

2. Separation between the longitudinal plating and bulkhead or web frame, in areas where the plating was prone to buckling (Figure 5b).

3. Poor printing of the single-perimeter plating at the areas connecting the hulls to the wet deck. This was caused by a combination of the single-perimeter printing, the fact that the wall was generated on top of support material, and the fact that one of the ends was completely free (Figure 5a).

As would be expected, the single-perimeter areas were also significantly more sensitive than other regions and sometimes suffered further damage during handling. Issues described above either resulted in discarding and reprinting the section at hand or were repaired before use, depending on the severity. Judging from the behaviour of the neighbouring double-perimeter regions, it was concluded that most of these issues would have been absent if at least 2 perimeters were used everywhere. Single-perimeter thicknesses will be avoided in future iterations of 3D-printed fully elastic models.

After printing, the mass of each section was measured and compared to expectations, showing maximum deviations of up to 1-2%. The largest deviations consistently corresponded to some of the lighter sections, indicating that the accuracy of the scales used was partly to blame. Extensive thickness measurements (more than 340 in total) were also taken. These indicated slightly higher values than anticipated: an average of 0.58 mm with a standard deviation of 0.04 mm. This is attributed to the way thicknesses are calculated and processed with slicing software for 3D printing, where two perimeters do not necessarily produce exactly double the thickness of a single perimeter. It should be pointed out that these measurements were all taken at various parts of the longitudinal structure, as the bulkheads and deep frames were all inaccessible.

After printing, the ballast masses were glued inside the structure with black kit. The sections were joined using epoxy, and then waterproofing of the model was performed by applying two layers of epoxy externally. Testing this method on a small specimen with the same thickness demonstrated consistently watertight behaviour. The exact thickness of the coating is very challenging to measure, but it increased the mass of the model by 300 g and is expected to have a more significant effect on the stiffness.

4. Discussion on verification and validation

4.1. Modal testing

Modal testing was performed both in air and in water (Figure 6). An instrumented hammer was used to generate the excitation force and 15 accelerometers were distributed throughout the main deck, resulting in a single-input-multiple-output configuration (SIMO). One of the main motivations behind the SIMO configuration was that there were few locations in the vessel were a hammer hit could be administered without risking local damage.
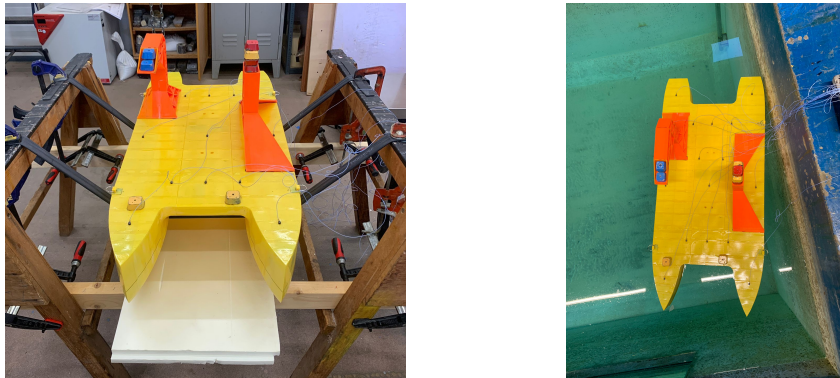

Figure 6. Hammer testing of the model in air (left) and in water (right).

For the tests in air, the model had to be suspended to emulate free boundary conditions. Attaching springs on the top deck was not an option, once more due to the risk of local damage. Consequently, bottom suspension was needed. Bungee cords were the first option, as used in previous tests with elastic models [8]. However, concerns were raised regarding the capability of the structure to withstand such concentrated pressure. Eventually, bicycle inner tubes were used instead, which combined low stiffness with a larger contact area. The experiments in air proved fruitless nonetheless: despite the low stiffness of the flexible supports, it was impossible to suspend the model without significantly affecting the structural responses, as the modes were primarily transverse. In fact, even seemingly artificial modes were observed, which are thought to have been introduced through the additional stiffness in the transverse direction.

A further indication of the artificial character of some modes came from the tests in water, as the mode shapes became significantly clearer and more similar to the ones observed in ANSYS simulations. Two significant issues remained, however:

- The magnitude of the added mass effects for the mode shapes at hand is less predictable than for vertical bending, rendering the comparison to the "dry" natural frequencies from ANSYS impossible without first performing hydrodynamic simulations.
- The simulations in ANSYS had already demonstrated clearly that, for such a complex structure with mode shapes combining several directions of response, even a slight change in the inertia properties can significantly affect the mode shapes.

Consequently, further work should be performed, primarily on developing a support system for tests in vacuo that does not cause interference, and secondarily on calculating the wet modes and corresponding natural frequencies. Modal testing using a shaker would be beneficial too, as some of the more dominant modes tend to mask the others in the frequency response during hammer testing.

4.2. Calibration

Calibration of a backbone model is relatively straightforward. Due to its large length and often uniform cross section, the backbone can be modelled as a uniform beam. Moreover, its material (usually steel or aluminium) behaves in the identical linear manner statically and dynamically. Consequently it is easy to perform a static test, perhaps by applying simply supported boundary conditions and a point load, and translating the measured strains to bending moments. In the current study, such a conversion is significantly more challenging. First of all, the model's mode shapes are clearly not beam-like, so the selection of appropriate analytical formulas for the conversion is complicated. Additionally, it has been demonstrated that 3D printed structures, even if plastics are used, can demonstrate very different moduli under static and dynamic excitation, although no further frequency dependence was identified [10]. Although in the past calibration has been performed using static tests, with reasonably acceptable results, a dynamic method is necessary to improve accuracy. Using a shaker for a harmonic point load could solve that part of the problem, but appropriate formulas to calculate bending moments need to be determined.

5. Conclusions

Hydroelastic experiments are usually performed using segmented models, where the hull consists of rigid segments, linked longitudinally by an appropriate stiffness source. In this work, additive manufacturing is used to produce a fully elastic model of a catamaran, including substantial internal structural detail. One major advantage of this methodology is that the model is flexible in all directions, and not just longitudinally, allowing mode shapes of the wet deck to be excited. The design and production procedures are described thoroughly, to allow replication in future work. The challenges during the design and manufacturing process are discussed in detailed, both in terms of scaling difficulties and issues due to the small wall thickness. Difficulties in the verification of the model are explained, and future steps aiming to overcome these issues are presented.

References

[1] Bishop RED, Price WG. On the scaling of flexible ship models. Journal of Sound and Vibration. 1980;73(3):345–352.

[2] Dessi D. Experimental analysis of the wave-induced response of a fast monohull via a segmented-hull model. Proceedings of the 7th International Conference on Fast Sea Transportation. 2003;7.

[3] Lavroff J, Davis MR, Holloway DS, Thomas G. Wave slamming loads on wave-piercer catamarans operating at high-speed determined by hydro-elastic segmented model experiments. Marine Structures. 2013;33:120–142.

[4] Watanabe I, Ueno M, Sawada H. Effects of Bow Flare Shape to the Wave Loads of a container ship. Journal of the Society of Naval Architects of Japan. 1989;1989(166):259–266.

[5] Wu YS, Chen RZ, Lin JR. Experimental technique of hydroelastic ship model. In: Proceedings of the Third International Conference on Hydroelasticity, Oxford, UK, September; 2003. p. 15–17.

[6] Grammatikopoulos A. A review of physical flexible ship models used for hydroelastic experiments. Marine Structures. 2023;90.

[7] Houtani H, Komoriyama Y, Matsui S, Oka M, Sawada H, Tanaka Y, et al. Designing a hydro-structural model ship to experimentally measure its vertical-bending and torshional vibrations. Journal of Advanced Research in Ocean Engineering. 2018;4(4):174–184.

[8] Grammatikopoulos A, Banks J, Temarel P. Prediction of the vibratory properties of ship models with realistic structural configurations produced using additive manufacturing. Marine Structures. 2020;73.

[9] Grammatikopoulos A, Banks J, Temarel P. The design and commissioning of a fully elastic model of a uniform container ship. Marine Structures. 2021;78.

[10] Grammatikopoulos A, Banks J, Temarel P. Experimental dynamic properties of ABS cellular beams produced using additive manufacturing. In: ECCM18 - 18th European Conference on Composite Materials. Athens, Greece; 2018. .

Bibliography

[1] J. Jin, Z. Jiang, S. Ringdalen Vatne, and Z. Ren, "Installation of pre-assembled offshore wind tur-bines using a catamaran vessel and an active gripper motion control method," *Grand Renewable Energy*, 2018. DOI: `10.24752/gre.1.0_156`.

[2] G. K. Kapsenberg, "On the slamming of ships. development of an approximate slamming predic-tion method," Ph.D. dissertation, 2018.

[3] G. Thomas, M. Davis, D. Holloway, and T. Roberts, "Transient dynamic slam response of large high speed catamarans," Oct. 2003.

[4] G. Thomas, M. R. Davis, D. S. Holloway, and T. Roberts, "The effect of slamming and whipping on the fatigue life of a high-speed catamaran," *Australian Journal of Mechanical Engineering*, vol. 3, no. 2, pp. 165–174, 2006. DOI: `10.1080/14484846.2006.11464505`.

[5] R. J. Shahraki, "The influence of hull form on the slamming behaviour of large high-speed cata-marans," Ph.D. dissertation, 2014.

[6] A. Grammatikopoulos, "A review of physical flexible ship models used for hydroelastic experi-ments," *Marine Structures*, vol. 90, p. 103 436, 2023. DOI: `10.1016/j.marstruc.2023.103436`.

[7] A. Marón and G. Kapsenberg, "Design of a ship model for hydro-elastic experiments in waves," *International Journal of Naval Architecture and Ocean Engineering*, vol. 6, no. 4, pp. 1130–1147, 2014, ISSN: 2092-6782. DOI: `https://doi.org/10.2478/IJNAOE-2013-0235`.

[8] J. Lavroff, M. R. Davis, D. S. Holloway, and G. Thomas, "Determination of wave slamming loads on high-speed catamarans by hydroelastic segmented model experiments," *International Journal of Maritime Engineering*, vol. 153, no. A3, 2011. DOI: `10.3940/rina.ijme.2011.a3.211`.

[9] A. Grammatikopoulos, J. Banks, and P. Temarel, "The design and commissioning of a fully elastic model of a uniform container ship," *Marine Structures*, vol. 78, p. 103 014, 2021. DOI: `10.1016/j.marstruc.2021.103014`.

[10] POLY-SERVICE, *Poly-pox thv 500 - harder 355 informatie*, Accessed (22/9/2023). [Online]. Avail-able: `https://www.polyservice.nl/content/25-technische-informatiebladen`.

[11] A. Grammatikopoulos, J. Banks, and P. Temarel, "Prediction of the vibratory properties of ship models with realistic structural configurations produced using additive manufacturing," *Marine Structures*, vol. 73, p. 102 801, 2020. DOI: `10.1016/j.marstruc.2020.102801`.